Bayesian Inference for Damage Identification based on Analytical Probabilistic Model

of Scattering Coefficient Estimators and Ultrafast Wave Scattering Simulation Scheme

Wang-Ji Yan*[1,2], Dimitrios Chronopoulos[2], Costas Papadimitriou[3], Sergio Cantero-Chinchilla[2,4], Guo-Shu Zhu[5]

[1]*State Key Laboratory of Internet of Things for Smart City and Department of Civil and Environmental Engineering, University of Macau, People's Republic of China*
[2]*Institute for Aerospace Technology & The Composites Group, The University of Nottingham, United Kingdom*
[3]*Department of Mechanical Engineering, University of Thessaly, Greece*
[4]*Aernnova Engineering Division S.A., Madrid 28034, Spain*
[5]*Department of Civil and Hydraulic Engineering, Hefei University of Technology, Hefei, Anhui, People's Republic of China*

Abstract: Ultrasonic Guided Waves (GW) actuated by piezoelectric transducers installed on structures have proven to be sensitive to small structural defects, with acquired scattering signatures being dependent on the damage type. This study presents a generic framework for probabilistic damage characterization within complex structures, based on physics-rich information on ultrasound wave interaction with existent damage. To this end, the probabilistic model of wave scattering properties estimated from measured GWs is inferred based on absolute complex-valued ratio statistics. Based on the probabilistic model, the likelihood function connecting the scattering properties predicted by a computational model containing the damage parametric description and the scattering estimates is formulated within a Bayesian system identification framework to account for measurement noise and modeling errors. The Transitional Monte Carlo Markov Chain (TMCMC) is finally employed to sample the posterior probability density function of the updated parameters. However, the solution of a Bayesian inference problem often requires repeated runs of "expensive-to-

1   evaluate" Finite Element (FE) simulations, making the inversion procedure firmly demanding

2   in terms of runtime and computational resources. To overcome the computational challenges

3   of repeated likelihood evaluations, a cheap and fast Kriging surrogate model built and based

4   on a set of training points generated with an experiment design strategy in tandem with a

5   hybrid Wave and Finite Element (WFE) computational scheme is proposed in this study. In

6   each "numerical experiment", the training outputs (i.e. ultrasound scattering properties) are

7   efficiently computed using the hybrid WFE scheme which combines conventional FE analysis

8   with periodic structure theory. By establishing the relationship between the training outputs

9   and damage characterization parameters statistically, the surrogate model further enhances the

10   computational efficiency of the exhibited scheme. Two case studies including one numerical

11   example and an experimental one are presented to verify the accuracy and efficiency of the

12   proposed algorithm.

13   **Key words**: Ultrasonic Guided Waves; Damage Identification; Bayesian Analysis; Wave

14   Finite Elements; Uncertainty Quantification; Surrogate Model

15

* Corresponding author.

E-mail address: civilyanwj@gmail.com (W.J. Yan); ezzdc1@exmail.nottingham.ac.uk (D. Chronopoulos); costasp@uth.gr (C. Papadimitriou); Sergio.CanteroChinchilla1@nottingham.ac.uk (S. Cantero-Chinchilla)

1

Nomenclature:

ω_k: the k-th frequency point;

$\Re_k$: the reflection coefficients at ω_k;

$\Im_k$: the transmission coefficients at ω_k;

$\boldsymbol{\theta}$: the damage characterization parameters;

$R_k(\boldsymbol{\theta})$: the reflection coefficients predicted by the structural damage model at $\boldsymbol{\theta}$;

$T_k(\boldsymbol{\theta})$: the transmission coefficients predicted by the structural damage model at $\boldsymbol{\theta}$;

λ: all model parameters to be identified;

$\mathcal{D}$: is the available data (i.e. the scattering property estimates);

$\mathfrak{M}$: the model class;

μ_{re} and μ_{tr}: the error terms of the reflection and transmission coefficients;

$p(\mathcal{D}|\mathfrak{M},\lambda)$: the likelihood function of the data $\mathcal{D}$;

$p(\lambda|\mathfrak{M})$: the prior PDF of the parameters;

$p(\lambda|\mathfrak{M},\mathcal{D})$: the posterior PDF;

$p(\mathcal{D}|\mathfrak{M})$: a normalization factor ensuring that the posterior PDF integrates to 1;

$x_{in}(t), x_{re}(t), x_{tr}(t)$: the incident, reflected and transmitted wave;

X_{in}, X_{re}, X_{tr}: FFT coefficients of the incident, reflected and transmitted wave;

n: the n-th time step of measurement;

N: the total number of time points for a wave;

$p_{\Re_k}(r_k)$: the PDF of the reflection coefficient $\Re_k$;

$p_{\Im_k}(\varepsilon_k)$: the PDF of the transmission coefficients $\Im_k$;

$\sigma_{in}^2, \sigma_{re}^2$ and σ_{tr}^2: the variances of X_{in}, X_{re} and X_{tr};

γ_{re} and γ_{tr}: the variances of the prediction errors μ_{re} and μ_{tr}.

$\mathbf{K}, \mathbf{C}$ and $\mathbf{M}$: the stiffness, viscous damping and mass matrices of the segment;

$\mathbf{q}$: the displacement and $\mathbf{f}$ denotes the forcing vectors;

$\mathbf{T}$: the symplectic transfer matrix in hybrid WFEM scheme;

$\mathbf{D}$: frequency dependent dynamic stiffness matrix;

$\mathbf{R}$: the rotation matrix of the waveguide;

$\mathbf{S}$: the scattering matrix predicted by the hybrid WFEM scheme;

Q: the vector of DoFs represented in the global coordinate system;

F: the vector of internal nodal forces in the global coordinate system;

$\boldsymbol{\Theta}$: vectors of independent input parameters;

$\boldsymbol{\theta}^{(i)}$: i-th sample generated by using the DoE strategy;

n_s: the number of DoE samples;

n_p: the number of damage characterization parameters to be identified;

$\mathbf{Y}_{n_s}(\boldsymbol{\Theta})$: a vector of training data outputs corresponding to $\boldsymbol{\Theta}$;

$\mathbf{Y}^{(i)}$: the i-th responses of the system corresponding to $\boldsymbol{\theta}^{(i)}$;

$\boldsymbol{\theta}^*$: arbitrary input vector;

$m(\boldsymbol{\theta}^*)$: the mean function at $\boldsymbol{\theta}^*$;

$\chi\left(\mathbf{\theta}^{*}\right)$: a zero-mean Gaussian process with unknown covariance function;

σ_{χ}^{2}: the process variance;

$Corr\left(\mathbf{\theta}^{(p)},\mathbf{\theta}^{(q)}\right)$: correlation function between training data $\mathbf{\theta}^{(p)}$ and $\mathbf{\theta}^{(q)}$;

ϑ_{j}: hyper-parameters;

$\hat{\eta}\left(\mathbf{\theta}^{*}\right)$ and $\hat{\sigma}\left(\mathbf{\theta}^{*}\right)$: mean and standard deviation of the Kriging model;

$\eta_{re}^{(k)}\left(\mathbf{\theta}^{*}\right)$ and $\eta_{tr}^{k}\left(\mathbf{\theta}^{*}\right)$: the scattering coefficients predicted by Kriging model;

1

2

1

1. Introduction

3　　The importance of Structural Health Monitoring (SHM), which involves performance

4　observation of a structure using response measurements, the extraction of damage-sensitive

5　features and the analysis of these features to assess structural health condition, has been

6　widely recognized [1,2]. One of the most fundamental tasks of SHM is implementing a

7　detection and characterization strategy for damage usually defined as changes to the material

8　and structural properties, which can adversely affect structural safety. Low-frequency damage

9　detection methods that utilize dynamic responses or dynamic properties have been applied

10　extensively in engineering structures and they have been proven to be useful in global

11　monitoring [3,4]. However, several researchers have reported that the damage detection

12　approaches based on the low-frequency characteristics are usually insensitive to small damage

13　[5].

14　　Nowadays, ultrasonic GW-based SHM methodologies have been widely reported to be

15　sensitive to small damage, convenient and efficient in detecting structural damage [6,7], such

16　as fatigue cracks in metallic structures, debonding and delamination in composite structures.

17　In real applications, actuators and sensors for damage identification using GWs are often

18　placed according to pitch-catch or pulse-echo configurations [8,9]. The scattered waves need

19　to be analyzed using certain damage identification algorithms to extract various characteristics

20　containing essential information about the damage [10]. Over the past decades, tremendous

efforts have been directed to extract structural conditions using GWs, and various algorithms

[10] including time-of-flight, time-reversal techniques, probability-based diagnostic imaging,

phased-array beamforming, and artificial intelligence techniques, etc. have been applied.

Though efforts have been devoted to damage detection using ultrasound GWs, there is

still significant room for further exploration in damage quantification and characterization due

to the lack of efficient techniques for predicting wave interaction with damage, especially for

composite structures. Layered structures typically have to be explicitly FE modelled with

individual elements per layer which results in unbearable computational times required to

obtain damage signatures [11]. More recently, scattering properties including reflection and

transmission coefficients have been viewed as promising candidates to provide a well

understanding of wave interaction with damage and to characterize structural damage [12,13].

It has been shown that the quantitative relationship between wave scattering and damage

intensity can be described by the scattering properties [14,15]. The physical background

behind this is given by the fact that elastic wave energy is transmitted, reflected and converted

to different wave modes when impinging to a structural inhomogeneity. On that basis, it is

possible to relate the damage extent or size to the acquired wave scattering properties [16].

Two approaches are normally utilized to calculate the scattering coefficients in the frequency

or time domain [17-19]. In the frequency domain, the coefficients as a function of frequency

can be computed by dividing the frequency responses of the reflected/transmitted wave signal

by that of the incident wave signal. In the time domain, these coefficients can be achieved by

taking the ratio of the value of the reflected/transmitted wave peak and that of the incident

1   wave peak after they are processed by the Hilbert transform. In this study, the relationships

2   between the damage and the scattering properties will be further exploited to formulate a

3   damage characterization procedure.

4   In the campaign of structural damage characterization, one critical issue that has been

5   widely accepted is that uncertainties due to endogenous factors, e.g. measurement noise,

6   model discrepancies, and external exogenous factors, such as environment variability and

7   measurement noises, should be appropriately considered [20,21]. Improving reliability and

8   robustness of damage detection approaches is uttermost important and to produce superior

9   methods, further research has to be produced explicitly accounting for these uncertainties

10   [22,23]. Bayesian statistics has been widely considered an excellent candidate for uncertainty

11   quantification in GW-based damage detection. A Bayesian approach was developed to

12   identify the damage location and wave velocity based on the time-of-flight (ToF) of the

13   scattered waves in each actuator-sensor path measured by a continuous wavelet transform

14   (CWT) [24]. A guided Bayesian inference approach was proposed to detect and quantify

15   multiple flaws in structures without a priori knowledge on the number of flaws by employing

16   the extended finite element method (XFEM) as the forward solver in the inverse detection

17   framework [25]. Ng and his co-workers have formulated Bayesian damage detection

18   framework by incorporating various technologies such as spectral finite element (SFE)

19   method, advanced signal processing techniques, etc. [26-29]. A Bayesian method was used to

20   characterize statistically the uncertain parameters in an ultrasonic inspection system from

21   limited signal measurements to enhance the confidence on the probability of detection curve

1 [30]. The sparse Bayesian learning approach was employed to detect structural damage by

2 Guided-wave signal processing and Gabor pulse model in [31]. A multilevel Bayesian inverse

3 problem framework was proposed in [32] to deal with these sources of uncertainty in the

4 context of ultrasound-based damage identification. Such calculations allow the quantification

5 of uncertainties associated with damage detection results, information that is essential for

6 making decisions about necessary remedial work [33]. Another essential feature of the

7 Bayesian statistical framework is that, if required, engineering judgment can be incorporated

8 into the damage characterization process to reduce the uncertainty of the results [34].

9   Bayesian statistics considers probability as a multi-valued propositional logic for

10 plausible reasoning [35,36], which is also viewed as a measure of the plausibility (a personal

11 degree of belief in a proposition) of a proposition conditioned on information [37,38]. By

12 making full use of the Bayesian system identification framework for accommodating

13 measurement noise and modeling errors properly, this study presents the first attempt to

14 formulate a generic methodology for probabilistic damage characterization based on wave

15 scattering characteristics. The scattering coefficients are probabilistically modelled by using

16 absolute complex ratio random variables. A Bayesian scheme makes inferences about the

17 damage characterization parameters directly by processing the statistical information

18 contained in the experimentally measured scattering properties. The Transitional Monte Carlo

19 Markov Chain (TMCMC) [39] is finally used to sample the posterior Probability Density

20 Function (PDF) of the updated parameters. Unfortunately, Bayesian inference based on GW

21 scattering properties is expensive and time-consuming because it requires repeated numerical

8

1 simulations. To address this critical issue, the hybrid WFE methodology is hereby employed

2 in order to efficiently simulate wave scattering when ultrasonic GW impinge a damaged

3 segment within a structure of arbitrary layering. It is shown that WFE predictions are several

4 orders of magnitudes faster than explicit FE modelling, even for 1D structures. Furthermore, a

5 cheap and fast Kriging surrogate model will be employed in tandem with the WFE scheme in

6 order to approximate the output as a function of model parameters. The Kriging predictor

7 provides a surrogate mapping between the probability spaces of the model predictions for the

8 scattering properties and the damage parameters in the likelihood evaluations. The procedure

9 is verified using numerical and experimental data in different damage configurations.

10   The manuscript of this study is organized as follows. Section 2 introduces the general

11 framework of probabilistic damage characterization with ultrasonic GW scattering properties,

12 while the challenges and solution strategy are also outlined. The Bayesian inference problem

13 for damage characterization parameters is formulated by incorporating a hybrid WFE scheme

14 within the surrogate approximation strategy in Section 3. Section 4 outlines the procedures of

15 Bayesian inference for probabilistic damage characterization based on scattering properties. In

16 Section 5, one numerical example is presented to illustrate the efficiency of the proposed

17 damage identification method. An experimental verification is also exhibited in this section

18 using a composite beam to further demonstrate the feasibility of the GW-based damage

19 characterization paradigm.

2. Theoretical Background, Challenges and Solution Strategies

An illustrative description of the envisaged considered system is presented in Fig. 1. The piezoelectric transducer excites propagating waves within the structure. The incoming GWs (+) impinge on the damaged structural segment and generate a set of outgoing (-) reflected and transmitted waves. The propagation of waves is often described in terms of "wave modes". Antisymmetric (A) and Symmetric (S) Lamb waves are typically employed as the most robust information vectors during ultrasonic GW monitoring, with the S_0 and A_0 wave types being the ones propagating in the low-frequency spectrum. For the purpose of clarity, the phase velocity dispersion curves are shown in Fig. 2 as an example, with each curve representing a wave mode. Shear, as well as torsional wave modes are also computed by the employed WFE scheme and are included in Fig. 1 (even though not to be excited within this study) for the sake of completeness.
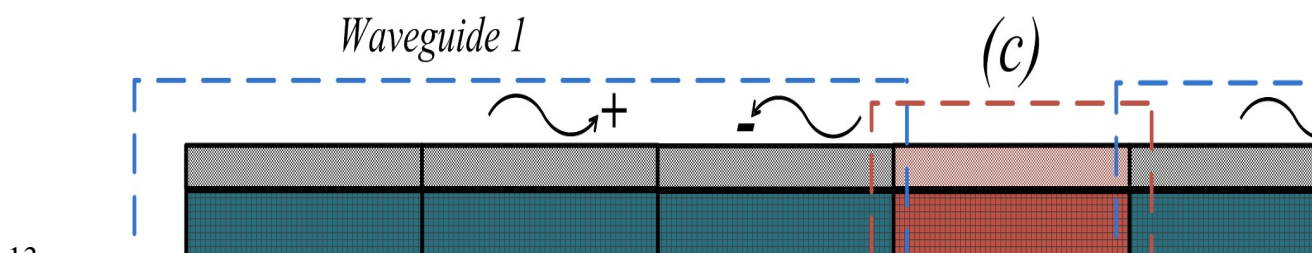
Fig. 1: Illustration of the UGW monitoring system: (a) the first part of the waveguide, (b) the second part of the waveguide, (c) damaged coupling element.
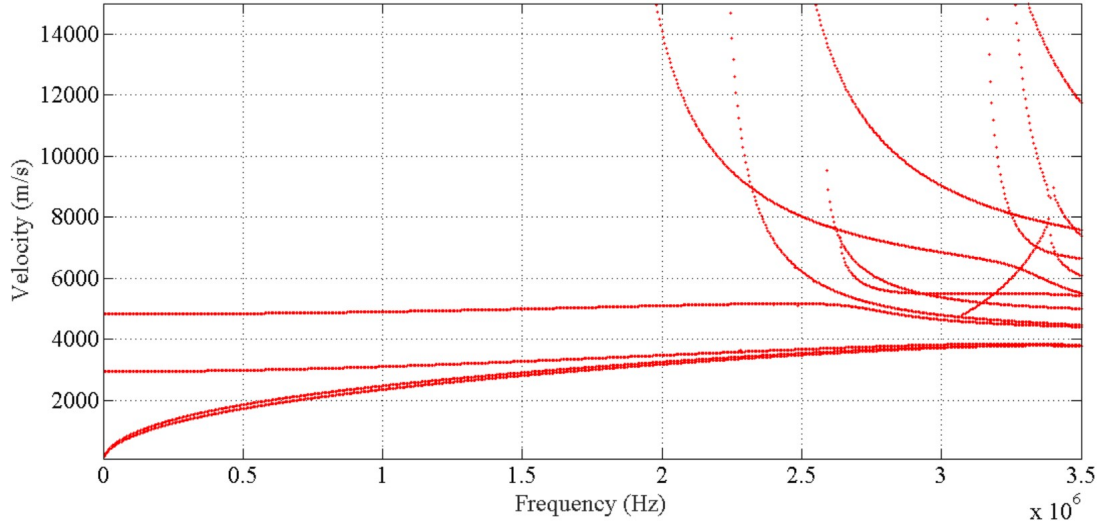
Fig. 2: Schematic of GW phase velocity curves for a layered structure computed with the WFE approach.

2.1 Bayesian formulation

In realistic applications, the scattering properties for different GW modes describe how much of a wave is reflected or transmitted by an impedance discontinuity in the transmission medium. Similar to the concept of frequency response function or transmissibility function in structural dynamics [40-42], the scattering coefficients are also defined as ratio functions in the frequency domain and they are functions of frequency ω_k. The reflection and transmission coefficients denoted by $\{\Re_k, \Im_k\}$ at ω_k are determined by dividing the frequency spectra of the reflected/transmitted signal by that of the incident wave signal. The reflection/transmission coefficients predicted by the structural damage model are denoted as $\{R_k(\boldsymbol{\theta}), T_k(\boldsymbol{\theta})\}$, defined by a set of damage parameters $\boldsymbol{\theta}$, which are to be identified. Each implemented damage scenario can be FE-modelled and the associated scattering coefficients can be numerically computed. The primary aim of this study is to make inferences about the damage

11

1 characterization parameters $\boldsymbol{\theta}$ by processing the information contained in scattering

2 coefficient measurements $\mathcal{D}=\{\mathfrak{R}_k,\mathfrak{I}_k\}$ within a Bayesian framework.

3   A Bayesian inference procedure is based on the well-known Bayes' theorem, with its

4 general formulation given as [35]:

$$p(\lambda|\mathfrak{M},\mathcal{D}) = \frac{p(\mathcal{D}|\mathfrak{M},\lambda) \cdot p(\lambda|\mathfrak{M})}{p(\mathcal{D}|\mathfrak{M})} = \frac{p(\mathcal{D}|\mathfrak{M},\lambda) \cdot p(\lambda|\mathfrak{M})}{\int_\Theta p(\mathcal{D}|\mathfrak{M},\lambda) \cdot p(\lambda|\mathfrak{M}) \cdot d\lambda} \qquad (1)$$

6 where λ denotes the value of the model parameters including the damage characterization

7 parameters $\boldsymbol{\theta}$ and prediction-error parameters, $\mathcal{D}$ is the available data (i.e. the scattering

8 property estimates), and $\mathfrak{M}$ is the model class.

9   Eq. (1) introduces a process to update prior knowledge on the parameters λ, by using data

10 $\mathcal{D}=\{\mathfrak{R}_k,\mathfrak{I}_k\}$ and conditional to some given model class $\mathfrak{M}$. The likelihood function

11 $p(\mathcal{D}|\mathfrak{M},\lambda)$ gives a measure of the agreement between the available experimental data

12 $\mathcal{D}=\{\mathfrak{R}_k,\mathfrak{I}_k\}$ and the corresponding numerical model output $\{R_k(\boldsymbol{\theta}),T_k(\boldsymbol{\theta})\}$. The posterior

13 distribution $p(\lambda|\mathfrak{M},\mathcal{D})$ expresses the updated knowledge about the parameters, providing

14 information on which parameter ranges are more probable based on the initial knowledge and

15 the measured scattering properties.

16   The statistical inference can be executed by embedding the "deterministic" structural

17 models within a class of probability models so that the structural models give a predictable

18 ("systematic") part and the prediction error is modeled as an uncertain ("random") part [43].

19 In the context of Bayesian inference with scattering coefficients, the measured outputs and the

20 numerical model outputs are connected as follows [43,44]:

$$\mathfrak{R}_k = R_k(\boldsymbol{\theta}) + \mu_{re} \qquad\qquad (2a)$$

$$\mathfrak{I}_k = T_k(\boldsymbol{\theta}) + \mu_{tr} \qquad\qquad (2b)$$

In Eq. (2), μ_{re} and μ_{tr} denote the error terms. It is worth mentioning here that μ_{re} and μ_{tr} are assumed to be zero-mean white noise with constant variances to be identified at each ω_k. Given that the measured scattering coefficients $\mathcal{D}=\{\mathfrak{R}_k,\mathfrak{I}_k\}$ follow a specific probability distribution, one can formulate the likelihood function $p(\mathcal{D}|\mathfrak{M},\lambda)$ by embedding Eq. (2) into the probabilistic model of $\mathcal{D}$.

The posterior distribution $p(\lambda|\mathfrak{M},\mathcal{D})$ can be achieved through a Laplace asymptotic approximation, which utilizes a Gaussian approximation as the posterior PDF. However, application of this approximation encounters difficulties when the amount of data is small, or the chosen class of models is unidentifiable. Also, such an approximation requires a non-convex optimization in a high-dimensional parametric space, which is computationally challenging, especially when the model class is not globally identifiable and there may be multiple global maxima [45]. In recent years, focus has shifted from analytical approximations to using stochastic simulation methods in which samples consistent with the posterior PDF $p(\lambda|\mathfrak{M},\mathcal{D})$ are generated. Stochastic simulation can handle more general cases than the asymptotic approximation approach [46]. In such methods, all probabilistic information encapsulated in $p(\lambda|\mathfrak{M},\mathcal{D})$ is characterized by posterior samples. MCMC simulation methods were among the most popular methods for solving the Bayesian inverse problem efficiently. In this study, the TMCMC algorithm [39] will be employed within a Bayesian inference for probabilistic damage characterization.

1   **2.2 Challenges and solution strategies**

2   Bayesian inference presents a mathematically rigorous approach for quantifying the

3   uncertainties of structural damage characterization parameters, which is useful for further risk

4   assessment. However, there are some challenges which may hinder its practical

5   implementation:

6   ● The likelihood function $p(\mathcal{D}|\mathfrak{M},\lambda)$ is obtained by embedding the "deterministic"

7   structural models within a class of probability models. Therefore, a probability model of

8   the measured outputs (i.e., $\mathcal{D}=\{\mathfrak{R}_k,\mathfrak{I}_k\}$) should be presented before implementing

9   Bayesian inference. As scattering coefficients are defined as the absolute ratios of fast

10   Fourier transform (FFT) of reflected/transmitted wave signal and incident wave signal,

11   one has to infer the statistics of the magnitude of a complex-valued random variable

12   composed of both real and imaginary parts.

13   ● In the procedure of Bayesian inference, one has to predict the scattering properties

14   $\{R_k(\boldsymbol{\theta}),T_k(\boldsymbol{\theta})\}$ repeatedly using physics-rich schemes containing the damage parameters

15   to be updated. For simple cases such as slender connected beams, analytical solutions of

16   the scattering coefficients are available. However, developing analytical models that

17   describe the dynamic behavior of more complicated structures comprised of various

18   damage scenarios can be a very challenging task. Therefore, one has to resort to

19   numerical simulations to compute the scattering coefficients accurately. The

14

computational cost is highly dependent on the number of FE runs and frequency bands selected for identification.

- The stochastic simulation approaches such as MCMC tools usually require a large number of numerical simulations. In each simulation, the scattering coefficients should be numerically evaluated by resorting to FE packages such as ANSYS and ABAQUS. In all iterative parameter updating methods, each iteration requires a FE analysis for the given set of updated parameters. If the structure of interest is composed of a large number of FEs (which is generally the case), the large number of computations involved in repeated FE runs can rule out many approaches due to the expense of carrying out an exhaustive number of runs. Worse still, stochastic simulation is usually implemented using proprietary programming language such as MATLAB, thus interfacing between different software environments such as MATLAB and ANSYS is an additional challenge, which may significantly limit their applicability for Bayesian uncertainty quantification.

To address the aforementioned challenges, the following strategies will be proposed:

➢ The complex Gaussian ratio distribution [40-42] has been employed to probabilistically model the statistics of ratio functions such as transmissibility functions and frequency response functions. In this study, the probabilistic distribution properties of the scattering coefficients estimates are also inferred based on the complex ratio statistics. Based on the probabilistic distribution of scattering coefficients, the likelihood function connecting the scattering properties predicted by the computational model containing the damage parameters to be updated and the scattering property estimates is formulated.

15

➤ An ultrafast hybrid WFE scheme will be employed to predict the scattering coefficients of a structural model with various types of damage [11,12]. Damage is modelled using standard FE methods whereas the waveguides are modelled using the WFE method. This relies on post-processing a standard FE model of a small segment of each waveguide using periodic structure theory. The degrees of freedom (DoF) at the interfaces of the WFE and FE models of the waveguides and the damage are compatible in order to avoid requirement for further computational treatment [47,48]. The models are coupled to yield the reflection and transmission matrices of the damage.

➤ To overcome the computational challenges of repeated likelihood evaluations and the difficulty of interfacing different software environments, complex numerical simulations for predicting scattering properties are replaced by a cheap and fast Kriging surrogate model built using an experiment design strategy in tandem with a hybrid WFE scheme. Kriging model approximates a function based on a set of training points and can eventually predict the function at new points. In each "numerical experiment", the training outputs (i.e. scattering properties) are efficiently computed using hybrid WFE. By establishing the relationship between the training outputs and damage identification parameters with a statistical method, the Kriging surrogate model obviates the need for a large number of repeated time-consuming FE runs. As a result, the WFE scheme is only required for training the outputs in the construction of the Kriging model, and is no longer involved in MCMC, thus significantly enhancing the efficiency of the presented methodology.

16

1   **3. Bayesian Inference for Damage Characterization**

2   **3.1 Scattering coefficient estimates and their probabilistic model**

3   *3.1.1 Scattering coefficient estimates*
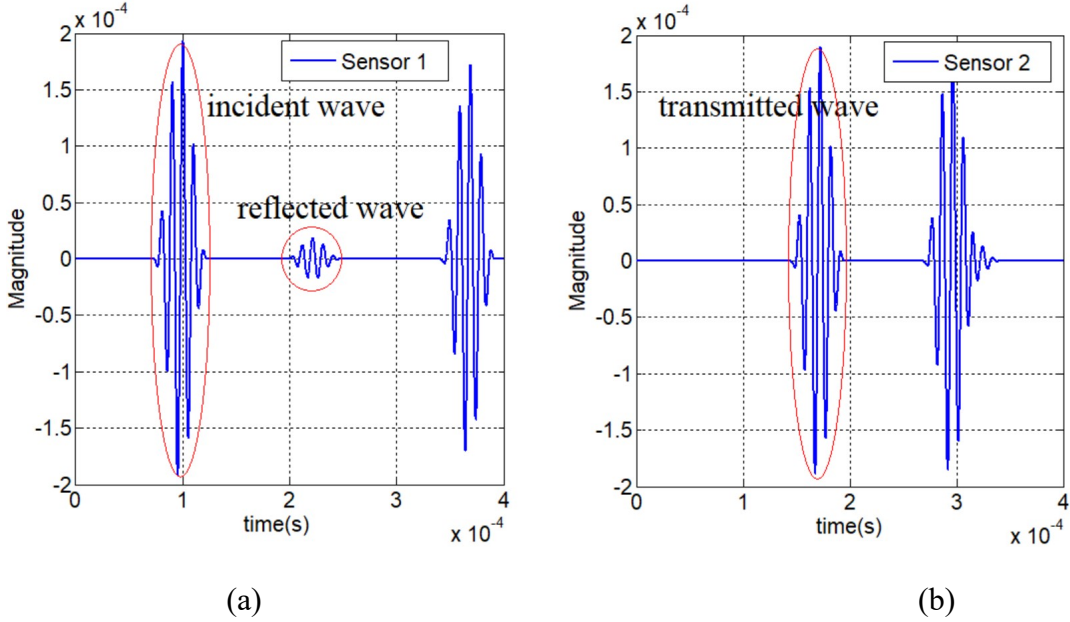
4

5   (a)   (b)

6   Fig. 3: A schematic of UGW signal measured at the left side and the right side of damage

7   segment: (a) incident and reflected wave; (b) transmitted wave.

8

9   As is illustrated in Fig. 1, the incident wave impinges on the damaged structural segment

10   and generates a set of reflected and transmitted waves. The propagation of waves is often

11   described in terms of different wave modes. Fig. 3 gives a schematic of the time series of the

12   incident wave, reflected wave and transmitted waves. The sampling time interval is assumed

13   to be Δt and the time duration for a specific mode is assumed to be T_d.

14   For a wave mode, the FFT coefficients of the reflected wave $x_{re}(t)$ at frequency ω_k in

15   rad/s are defined as:

1 $$X_{re}(\omega_k) = \sqrt{\frac{\Delta t}{2\pi N}} \sum_{n=0}^{N-1} x_{re}(n\Delta t) e^{(-\mathbf{i}\omega_k n\Delta t)}$$ (3)

2 where $n = 1, 2, \cdots, N$, $\mathbf{i}^2 = -1$, $\omega_k = k\Delta\omega$, $k = 1, 2, \cdots, Int(N/2)$. Similar operations can be

3 conducted for the transmitted wave $x_{tr}(t)$ and incident wave $x_{in}(t)$, and their corresponding

4 FFT coefficients are denoted by $X_{tr}(\omega_k)$ and $X_{in}(\omega_k)$, respectively.

5   In the field of wave propagation, the scattering coefficients can be estimated by taking

6 the absolute ratio of the FFT of reflected/transmissive wave and the FFT of the incident wave

7 as [17]:

8 $$\Re_k = \left| X_{re}(\omega_k) / X_{in}(\omega_k) \right|$$ (4a)

9 $$\Im_k = \left| X_{tr}(\omega_k) / X_{in}(\omega_k) \right|$$ (4b)

10 In this work, all "k" shown in the bracket, in the subscript or in the superscript denote

11 frequency ω_k.

12 ### 3.1.2 Probabilistic models of scattering coefficients

13 Assume that the variances of $X_{in}(\omega_k)$ and $X_{re}(\omega_k)$ are denoted by $\sigma_{in}^2(\omega_k)$ and $\sigma_{re}^2(\omega_k)$ while

14 their correlation coefficient is given by ρ_k. Using the new theorem on circularly-symmetric

15 complex Gaussian ratio distribution, one can prove that the PDF of $U_k = X_{re}(\omega_k) / X_{in}(\omega_k)$ is

16 given by [40]

17 $$p_{U_k}(u_k) = \pi^{-1}(1 - \rho_k^* \rho_k)\sigma_{in}^2 \sigma_{re}^2 \left[\sigma_{re}^2 - \left(u_k^* \rho_k^* + u_k \rho_k \right) \sigma_{in} \sigma_{re} + u_k u_k^* \sigma_{in}^2 \right]^{-2}$$ (5)

18 where $(\cdot)^*$ denotes the complex conjugate. It is worth reminding that "ω_k" is ignored here for

19 simplicity.

1   The complex-valued random variable $U_k = \Re_k e^{-i\Theta_k}$, expressed in the polar coordinate

2   system, and the PDF of the reflected coefficients $\Re_k$ is equal to

3
$$p_{\Re_k}(r_k) = \frac{2r_k \sigma_{in}^2 \sigma_{re}^2 \left(1 - \beta_k^2\right)\left(\sigma_{re}^2 + r_k^2 \sigma_{in}^2\right)}{\left[\left(\sigma_{re}^2 + r_k^2 \sigma_{in}^2\right)^2 - \left(2r_k \beta_k \sigma_{in} \sigma_{re}\right)^2\right]^{3/2}} \tag{6}$$

4   where β_k denote the magnitude of ρ_k. Assume that the correlation between $X_{in}(\omega_k)$ and

5    $X_{re}(\omega_k)$ are negligible, i.e. $\rho=0$, then (6) can be simplified as:

6
$$p_{\Re_k}(r_k) = \frac{2r_k \sigma_{in}^2 \sigma_{re}^2}{\left(\sigma_{re}^2 + r_k^2 \sigma_{in}^2\right)^2} \tag{7}$$

7   Similarly, if the variance of the transmitted wave is denoted by σ_{tr}^2, then one can obtain the

8   PDF of the transmission coefficients $\Im_k$ as follows:

9
$$p_{\Im_k}(\varepsilon_k) = \frac{2\varepsilon_k \sigma_{in}^2 \sigma_{tr}^2}{\left(\sigma_{tr}^2 + \varepsilon_k^2 \sigma_{in}^2\right)^2} \tag{8}$$

10   It is worth mentioning here again that Eq. (2), Eq. (7) and (8) will be used in Section 3.3 to

11   derive the likelihood function. The probabilistic models of the measured scattering

12   coefficients can connect the measured outputs and the model outputs properly so that the

13   inherent randomness of measurements and modelling errors are well accommodated.

14   **3.2 Scattering coefficients predicted by an ultrafast hybrid WFE scheme**

15   In the context of Bayesian inference problem, likelihood evaluation usually requires repeated

16   runs of "expensive-to-evaluate" explicit FE simulations to obtain physics-rich information

17   about the GW scattering coefficients. The likelihood evaluation makes the inversion

18   procedure firmly demanding in terms of runtime and computational resources. In this section,

1 hybrid WFE scheme will be employed to reduce the computational burden of conventional

2 full FEM analysis scheme by several orders of magnitude. Furthermore, a fast Kriging

3 surrogate model will be introduced in this section. The generation of the Kriging predictor

4 model requires a dedicated experiment design strategy for extracting the set of training points.

5 In each "computer experiment", the training outputs of the scattering properties are efficiently

6 computed through the hybrid WFE scheme. As a result, the relationship between the training

7 outputs and damage parameters is established statistically to avoid the need for an exhaustive

8 number of runs within the Bayesian inference.

9 *3.2.1 Hybrid WFEM scheme*
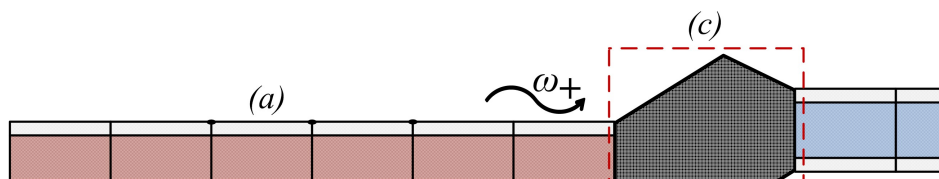
10

11 Fig. 4: Schematic of two waveguides attached at a damage segment with incident, reflected

12 and transmitted waves: (a) The first waveguide; (b) The second waveguide; (c) An arbitrary

13 coupling element (possibly containing damage) explicitly modelled with FEs.

14 A hybrid WFEM approach will hereby be employed for numerically determining the

15 reflection and transmission matrices for a given set of damage properties. The individual

16 intrinsic characteristics of a given damage scenario can be expressed in terms of its

17 frequency-dependent GW interaction signatures. Conveniently, different wave types have

18 different interaction properties with each damage scenario for each wavelength. Healthy,

19 periodic structures of arbitrary layering are hereby modelled as waveguides. The wave

20

1   behavior of such structures involves the propagation of elastic packets through the

2   waveguides which impinge and interact with structural inhomogeneities. In Fig.4, the

3   damaged segment is modelled using standard FE methods whereas the waveguides are

4   modelled using the WFE approach. This relies on post-processing a standard FE model of a

5   small segment for each waveguide using periodic structure theory. The DoF at the interfaces

6   of the WFE and FE models of the waveguides and the joint are compatible. The models are

7   coupled to yield the reflection and transmission matrices of the damage. The review presented

8   in this section is heavily borrowed from [12,13].
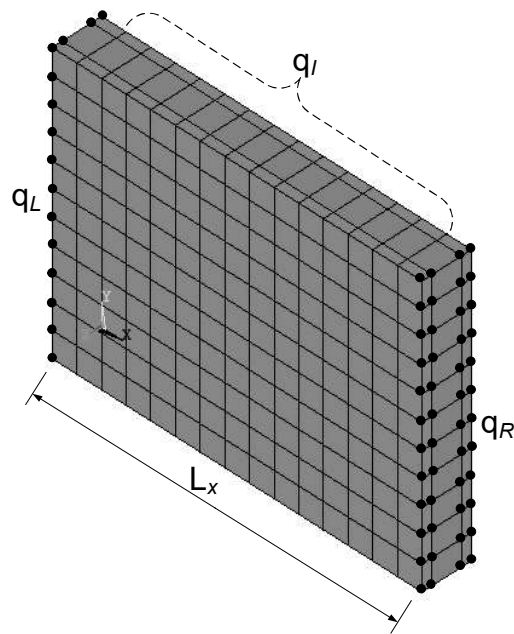
9

10   Fig. 5: Schematic of a periodic healthy waveguide discretized by 3D linear FE. The interface

11   left (q_L) and right (q_R) nodes are also depicted.

12   The cross-section of the waveguide can be arbitrarily complex, as shown in Fig. 5. The

13   WFE method starts with obtaining the FE model of a segment of the waveguide using any FE

14   package with the only constraint being that the nodes and their DoF are ordered identically on

21

1 the left and right sides of the segment. Internal nodes can be eliminated via dynamic

2 condensation or explicitly solved for the sake of enhanced accuracy. If the structure undergoes

3 time harmonic motion at frequency ω_k and in the absence of external forces, the nodal

4 displacements and forces are related through the frequency dependent Dynamic Stiffness

5 Matrix (DMS) of the segment:

6
$$\left(\mathbf{K} + i\omega_k\mathbf{C} - \omega_k^2\mathbf{M}\right)\mathbf{q} = \mathbf{f} \tag{9}$$

7 where $\mathbf{K}$, $\mathbf{C}$, and $\mathbf{M}$ are the stiffness, viscous damping and mass matrices, respectively;

8 $\mathbf{q}$ denotes the displacement and $\mathbf{f}$ denotes the forcing vectors. The frequency dependent

9 DMS of the waveguide's periodic segment can be partitioned with regard to its left/right sides

10 and internal DoF as [12,13]

11
$$\begin{bmatrix} \mathbf{D}_{LL} & \mathbf{D}_{LI} & \mathbf{D}_{LR} \\ \mathbf{D}_{IL} & \mathbf{D}_{II} & \mathbf{D}_{IR} \\ \mathbf{D}_{RL} & \mathbf{D}_{RI} & \mathbf{D}_{RR} \end{bmatrix} \begin{Bmatrix} \mathbf{q}_L \\ \mathbf{q}_I \\ \mathbf{q}_R \end{Bmatrix} = \begin{Bmatrix} \mathbf{f}_L \\ \mathbf{0} \\ \mathbf{f}_R \end{Bmatrix} \tag{10}$$

12 where L, R and I denote left/right sides and internal DoF.

13 Using a dynamic condensation for the internal DoF, the problem can be expressed as

14
$$\begin{bmatrix} \mathbf{D}_{LL} - \mathbf{D}_{LI}\mathbf{D}_{II}^{-1}\mathbf{D}_{IL} & \mathbf{D}_{LR} - \mathbf{D}_{LI}\mathbf{D}_{II}^{-1}\mathbf{D}_{IR} \\ \mathbf{D}_{RL} - \mathbf{D}_{RI}\mathbf{D}_{II}^{-1}\mathbf{D}_{IL} & \mathbf{D}_{RR} - \mathbf{D}_{RI}\mathbf{D}_{II}^{-1}\mathbf{D}_{IR} \end{bmatrix} \begin{Bmatrix} \mathbf{q}_L \\ \mathbf{q}_R \end{Bmatrix} = \begin{Bmatrix} \mathbf{f}_L \\ \mathbf{f}_R \end{Bmatrix} \tag{11}$$

15 Assuming that no external forces are applied on the segment, the displacement continuity and

16 force equilibrium equations at the interface of two consecutive periodic segments s and $s+1$

17 give:

18
$$\mathbf{q}_L^{s+1} = \mathbf{q}_R^s; \mathbf{f}_L^{s+1} = -\mathbf{f}_R^s \tag{12}$$

19 Using Eqs. (11) and (12) the relation of the displacements and forces of the left and right sides

1 of the segment can be written as:

2
$$\begin{Bmatrix} \mathbf{q}_L^{s+1} \\ \mathbf{f}_L^{s+1} \end{Bmatrix} = \mathbf{T} \begin{Bmatrix} \mathbf{q}_L^{s} \\ \mathbf{f}_L^{s} \end{Bmatrix} \qquad (13)$$

3 and the expression of the symplectic transfer matrix $\mathbf{T}$ can be written as

4
$$\mathbf{T} = \begin{bmatrix} \mathbf{D}_{11} & \mathbf{D}_{12} \\ \mathbf{D}_{21} & \mathbf{D}_{22} \end{bmatrix} \qquad (14)$$

5 where

6
$$\mathbf{D}_{11} = -(\mathbf{D}_{LR} - \mathbf{D}_{LI}\mathbf{D}_{II}^{-1}\mathbf{D}_{IR})^{-1}(\mathbf{D}_{LL} - \mathbf{D}_{LI}\mathbf{D}_{II}^{-1}\mathbf{D}_{IL}) \qquad (15a)$$

7
$$\mathbf{D}_{12} = (\mathbf{D}_{LR} - \mathbf{D}_{LI}\mathbf{D}_{II}^{-1}\mathbf{D}_{IR})^{-1} \qquad (15b)$$

8
$$\mathbf{D}_{21} = -\mathbf{D}_{RL} + \mathbf{D}_{RI}\mathbf{D}_{II}^{-1}\mathbf{D}_{IL} + (\mathbf{D}_{RR} - \mathbf{D}_{RI}\mathbf{D}_{II}^{-1}\mathbf{D}_{IR})(\mathbf{D}_{LR} - \mathbf{D}_{LI}\mathbf{D}_{II}^{-1}\mathbf{D}_{IR})^{-1}(\mathbf{D}_{LL} - \mathbf{D}_{LI}\mathbf{D}_{II}^{-1}\mathbf{D}_{IL}) \qquad (15c)$$

9
$$\mathbf{D}_{22} = -(\mathbf{D}_{RR} - \mathbf{D}_{RI}\mathbf{D}_{II}^{-1}\mathbf{D}_{IR})(\mathbf{D}_{LR} - \mathbf{D}_{LI}\mathbf{D}_{II}^{-1}\mathbf{D}_{IR})^{-1} \qquad (15d)$$

10 With a wave propagating freely along the x direction, the propagation constant

11 $\gamma = e^{-ikL_x}$ relates the right and left nodal displacements and forces by:

12
$$\mathbf{q}_R^{s} = \gamma\mathbf{q}_L^{s}; \mathbf{f}_R^{s} = -\gamma\mathbf{f}_L^{s} \qquad (16)$$

13 By substituting Eqs. (12) and (16) into Eq. (13), the free wave propagation is described by the

14 eigenproblem [12,13]:

15
$$\gamma \begin{Bmatrix} \mathbf{q}_L^{s} \\ \mathbf{f}_L^{s} \end{Bmatrix} = \mathbf{T} \begin{Bmatrix} \mathbf{q}_L^{s} \\ \mathbf{f}_L^{s} \end{Bmatrix} \qquad (17)$$

16 whose eigenvalue γ_{ω_k} and eigenvectors $\mathbf{\Phi}_{\omega_k} = \begin{Bmatrix} \mathbf{\Phi}_q \\ \mathbf{\Phi}_f \end{Bmatrix}_{\omega_k}$ solution sets provide a comprehensive

17 description of the propagation constants and the wave mode shapes for each of the elastic

18 waves propagating in the structural waveguide at a specified angular frequency ω_k. Both

19 positive going waves (with $\gamma_{\omega_k}^{+}$ and $\mathbf{\Phi}_{\omega_k}^{+}$) and negative going waves ($\gamma_{\omega_k}^{-}$ and $\mathbf{\Phi}_{\omega_k}^{-}$) are sought

1 through the eigen-solution. Positive going waves are characterized by [12,13]:

$$2 \qquad \begin{cases} |\gamma_{\omega_k}^+| \le 1 \\ \Re eal\left(i\omega_k \Phi_f^{+T} \Phi_q^+\right) < 0, \quad \text{if } |\gamma_{\omega_k}^+| = 1 \end{cases} \qquad (18)$$

3 stating that when a wave is travelling in the positive x direction its amplitude should be

4 decreasing, or that if its amplitude remains constant (in the case of propagating waves with

5 complete absence of attenuation), then there is time averaged power transmission in the

6 positive direction.

7   The wave scattering at the inhomogeneity (damage) will next be considered. Assume

8 waveguides are attached at a joint structural element containing an arbitrary inhomogeneity as

9 shown in Fig. 4. The waveguides are modelled using the WFE method described above and

10 the damage is modelled using standard FE description which allows for arbitrary complexity.

11 Time harmonic behavior of the damage coupling FE part is described through [12,13]

$$12 \qquad \begin{bmatrix} \tilde{\mathbf{D}}_{ii} & \tilde{\mathbf{D}}_{in} \\ \tilde{\mathbf{D}}_{ni} & \tilde{\mathbf{D}}_{nn} \end{bmatrix} \begin{Bmatrix} \mathbf{Q}_i \\ \mathbf{Q}_n \end{Bmatrix} = \begin{Bmatrix} \mathbf{F}_i \\ \mathbf{F}_n \end{Bmatrix} \qquad (19)$$

13 where $\mathbf{Q}$ and $\mathbf{F}$ are vectors of DoFs and internal nodal forces represented in the global

14 coordinate system and the subscripts i and n represent interface and non-interface nodes,

15 respectively. Since it is assumed that no external forces are applied at the non-interface nodes

16 then $F_n = 0$ and the FE model of the joint can be condensed as [12,13]

$$17 \qquad \mathbf{D}_{ii} \mathbf{Q}_i = \mathbf{F}_i \qquad (20a)$$

$$18 \qquad \mathbf{D}_{ii} = \tilde{\mathbf{D}}_{ii} - \tilde{\mathbf{D}}_{in} \tilde{\mathbf{D}}_{nn}^{-1} \tilde{\mathbf{D}}_{ni} \qquad (20b)$$

$$19 \qquad \mathbf{Q}_n = -\tilde{\mathbf{D}}_{nn}^{-1} \tilde{\mathbf{D}}_{ni} \mathbf{Q}_i \qquad (20c)$$

20 After straightforward manipulation, the scattering matrix follows as [12,13]:

1 $$\mathbf{S} = -\left[\mathbf{R}\boldsymbol{\Phi}_f^- - \mathbf{D}_{ii}\mathbf{R}\boldsymbol{\Phi}_q^-\right]^{-1}\left[\mathbf{R}\boldsymbol{\Phi}_f^+ - \mathbf{D}_{ii}\mathbf{R}\boldsymbol{\Phi}_q^+\right] \qquad (21)$$

2 where $\mathbf{R}$ denotes the rotation matrix of the waveguide transforming the DoF from the local

3 coordinate system to the global coordinate system; $\mathbf{R}$ being block-diagonal. As a result, the

4 scattering properties including the reflection, transmission and conversion coefficients for

5 different modes can be directly obtained from Eq. (21). One can refer to [12,13] for more

6 information about the strategy.

7 *3.2.2 Kriging surrogate model in tandem with hybrid WFEM scheme*

8 Surrogates are metamodels representing a functional relation between the inputs (i.e., damage

9 parameters to be identified in this study) and the model outputs (i.e., ultrasonic GW scattering

10 coefficients in this study). While there is a plethora of approaches, the most commonly used

11 metamodels are based on linear or polynomial regression, on a least-squares formulation or on

12 Kriging and radial basis functions. Compared to the conventional response surface method

13 requiring an understanding of the qualitative tendency of the entire design space, the Kriging

14 model provides better flexibility of modelling response data with multiple local extreme

15 values [49,50]. In engineering, Kriging is widely used because it is fast to train and is

16 generally more accurate than other types of surrogate models. Originating from geographical

17 space statistics [49], Kriging model is a data interpolation scheme to predict unknown values

18 from data at known locations. Kriging is also known as Gaussian process or Bayesian

19 emulator. As a virtually unbiased minimum variance estimation model, the local estimation

20 characteristics of the Kriging model can predict the function value distribution satisfactorily

21 by means of a correlation function. With the development of the Kriging toolbox based on

1   MATLAB-DACE [51], the Kriging model has been extensively applied in various fields

2   structural optimization [52], reliability engineering [53,54], and structural model updating

3   [55,56].

4   Table 1: Procedures of constructing surrogate model for predicting scattering coefficients

Step	Procedures
1	Establish the damage model and the model parameters $\boldsymbol{\theta} \in \mathbb{R}^{n_p}$ to be identified
2	Formulate the hybrid WFEM as introduced in Section 3.2.1
3	Use DoE to generate n_s sampling inputs $\boldsymbol{\Theta} = \{\boldsymbol{\theta}^{(1)}, \boldsymbol{\theta}^{(2)} \cdots \boldsymbol{\theta}^{(n_s)}\}^T$

4	Calculate training data outputs at different ω_k:
	for $k = 1 : n_f$
	  for $i = 1 : n_s$
	    ● Compute the reflection and transmission coefficients $\mathbf{Y}_{re}^{(i)}(\omega_k)$ and $\mathbf{Y}_{tr}^{(i)}(\omega_k)$ at each input $\boldsymbol{\theta}^{(i)}$ using hybrid WFE scheme.
	  end
	end

5	for $k = 1 : n_f$ ● Organize training data $\mathcal{D}_{re}(\omega_k) = (\boldsymbol{\Theta}, \mathbf{Y}_{re}(\omega_k))$ and $\mathcal{D}_{tr}(\omega_k) = (\boldsymbol{\Theta}, \mathbf{Y}_{tr}(\omega_k))$ with $\mathbf{Y}_{re}(\omega_k) = \left[\mathbf{Y}_{re}^{(1)}(\omega_k), \mathbf{Y}_{re}^{(2)}(\omega_k), \cdots, \mathbf{Y}_{re}^{(n_s)}(\omega_k)\right]$ and $\mathbf{Y}_{tr}(\omega_k) = \left[\mathbf{Y}_{tr}^{(1)}(\omega_k), \mathbf{Y}_{tr}^{(2)}(\omega_k), \cdots, \mathbf{Y}_{tr}^{(n_s)}(\omega_k)\right]$. End

6	Formulate Kriging model for reflection/transmission coefficients at different ω_k:
	for $k = 1 : n_f$
	  ● Construct Kriging model $R_k = \eta_{re}^{(k)}(\boldsymbol{\theta}^*)$ from $\mathcal{D}_{re}(\omega_k) = (\boldsymbol{\Theta}, \mathbf{Y}_{re}(\omega_k))$ to characterize the relationship between the reflection coefficients and $\boldsymbol{\theta}$;
	  ● Construct Kriging model $T_k = \eta_{tr}^{k}(\boldsymbol{\theta}^*)$ from $\mathcal{D}_{tr}(\omega_k) = (\boldsymbol{\Theta}, \mathbf{Y}_{tr}(\omega_k))$ to characterize the relationship between the transmission coefficients and $\boldsymbol{\theta}$.
	End

5   *Here $n_f = k_2 - k_1 + 1$ denotes the number of frequency points within the frequency band.

6   To formulate a Kriging predictor model, it requires initial Design of Experiments (DoE).

7   These samples are frequently referenced as the training set or support points. Appropriate

8   DoE plays a vital role in constructing a high-fidelity Kriging model because DoE influences

1   the creation of the most informative training data. A common choice for the training design is

2   the Latin Hypercube Design (LHD), which guarantees to spread design points evenly across

3   each input parameter dimension. With the training set at hand, one can then calculate the

4   predicted values of the surrogate model at various sample points in the parameter space by

5   performing an "experiment" at each of those samples based on the hybrid WFE scheme

6   introduced in Section 3.2.1. A number of output values obtained from the "experiment"

7   running across the parameter domain are employed to fit a Kriging model using the DACE

8   toolbox [51].

9   We assume that vectors of independent input parameters $\mathbf{\Theta}=\left\{\mathbf{\theta}^{(1)},\mathbf{\theta}^{(2)}\cdots\mathbf{\theta}^{(n_s)}\right\}^{T}$ with

10   $\mathbf{\theta}^{(i)}\in\mathbb{R}^{n_p\times1}$ are selected by using the LHD strategy. Here n_s and n_p denote the number of DoE

11   samples and the number of damage characterization parameters to be identified. The hybrid

12   WFE introduced in Section 3.2.1 is run at each point $\mathbf{\theta}^{(i)}$ in the training design, yielding a

13   vector of training data outputs $\mathbf{Y}_{n_s}\left(\mathbf{\Theta}\right)=\left[\mathbf{Y}^{(1)},\mathbf{Y}^{(2)}\cdots\mathbf{Y}^{(n_s)}\right]$ with $\mathbf{Y}^{(i)}\in\mathbb{R}^{n_p\times1}$ denoting responses

14   of the system, i.e. the scattering coefficients in this study. A Kriging predictor for the output

15   data consists of a second order polynomial and a random function. For any input vector $\mathbf{\theta}^{*}$,

16   the Kriging predictor model consists of a Gaussian process η that is expressed as [50,53]

17   $$\eta\left(\mathbf{\theta}^{*}\right)=m\left(\mathbf{\theta}^{*}\right)+\chi\left(\mathbf{\theta}^{*}\right) \tag{22}$$

18   where $m\left(\mathbf{\theta}^{*}\right)$ denotes the mean function, which is an optional regression model

19   estimated from available data; $\chi\left(\mathbf{\theta}^{*}\right)$ is usually assumed to be a Gaussian stationary

20   process with zero mean and unknown covariance. The covariance matrix of $\chi\left(\mathbf{\theta}^{*}\right)$ can be

21   modeled as [53]

$$\text{Cov}\left(\chi(\boldsymbol{\theta}^{(p)}), \chi(\boldsymbol{\theta}^{(q)})\right) = \sigma_\chi^2 Corr\left(\boldsymbol{\theta}^{(p)}, \boldsymbol{\theta}^{(q)}\right), \quad p, q = 1, 2, \cdots, n_s \tag{23}$$

where σ_χ^2 is the process variance and $Corr\left(\boldsymbol{\theta}^{(p)}, \boldsymbol{\theta}^{(q)}\right)$ is a parametric correlation function. A classical common choice for this correlation function is the exponential correlation function which permits control of both the range of influence and the smoothness of the approximation function [53]:

$$Corr\left(\boldsymbol{\theta}^{(p)}, \boldsymbol{\theta}^{(q)}\right) = \prod_{j=1}^{n_p} \exp\left(-\vartheta_j \left|\boldsymbol{\theta}_j^{(p)} - \boldsymbol{\theta}_j^{(q)}\right|^\delta\right), \quad 0 < \delta \le 2 \tag{24}$$

while ϑ_j are scale factors that can be estimated using maximum likelihood. Kriging provides an optimal unbiased linear predictor at any $\boldsymbol{\theta}^*$ as [53]

$$\hat{\eta}\left(\boldsymbol{\theta}^*, \boldsymbol{\Theta}\right) = m\left(\boldsymbol{\theta}^*\right) + \mathbf{r}\left(\boldsymbol{\theta}^*, \boldsymbol{\Theta}\right)^{\mathrm{T}} \tilde{\mathbf{R}}^{-1}\left(\boldsymbol{\Theta}\right)\left(\mathbf{Y}_{n_s}\left(\boldsymbol{\Theta}\right) - \mathbf{m}_{n_s}\left(\boldsymbol{\Theta}\right)\right) \tag{25}$$

where $\tilde{\mathbf{R}}_{pq}\left(\boldsymbol{\Theta}\right) = Corr\left(\boldsymbol{\theta}^{(p)}, \boldsymbol{\theta}^{(q)}\right)$; $\mathbf{r}\left(\boldsymbol{\theta}^*, \boldsymbol{\Theta}\right) = \left[Corr\left(\boldsymbol{\theta}^*, \boldsymbol{\theta}^{(1)}\right), \cdots, Corr\left(\boldsymbol{\theta}^*, \boldsymbol{\theta}^{(n_s)}\right)\right]^{\mathrm{T}}$;

$\mathbf{m}_{n_s}\left(\boldsymbol{\Theta}\right) = \left[m\left(\boldsymbol{\theta}^{(1)}\right) \cdots m\left(\boldsymbol{\theta}^{(n_s)}\right)\right]$; $\mathbf{Y}_{n_s}\left(\boldsymbol{\Theta}\right) = \left[\mathbf{Y}^{(1)}, \mathbf{Y}^{(2)} \cdots \mathbf{Y}^{(n_s)}\right]$.

Moreover, using Gaussian processes makes it possible to compute confidence intervals for the prediction through the variance [53]

$$\hat{\sigma}^2\left(\boldsymbol{\theta}^*, \boldsymbol{\Theta}\right) = \hat{\sigma}_\chi^2\left(1 - \mathbf{r}\left(\boldsymbol{\theta}^*, \boldsymbol{\Theta}\right)^{\mathrm{T}} \tilde{\mathbf{R}}^{-1}\left(\boldsymbol{\Theta}\right)\mathbf{r}\left(\boldsymbol{\theta}^*, \boldsymbol{\Theta}\right)\right) \tag{26}$$

Ultimately, the Kriging predictor $\eta\left(\boldsymbol{\theta}^*\right)$ leads to an estimate that is a Gaussian random variable with mean $\hat{\eta}\left(\boldsymbol{\theta}^*\right)$ and standard deviation $\hat{\sigma}\left(\boldsymbol{\theta}^*\right)$, that is

$$\eta\left(\boldsymbol{\theta}^*\right) \sim \mathbb{N}\left(\hat{\eta}\left(\boldsymbol{\theta}^*, \boldsymbol{\Theta}\right), \hat{\sigma}\left(\boldsymbol{\theta}^*, \boldsymbol{\Theta}\right)\right) \tag{27}$$

It is worth noting that the scattering coefficients are vector-valued functions in terms of frequency ω_k, which inevitably change when frequency varies. Therefore, the relationship

1   between the model output and parameters $\boldsymbol{\theta}^*$ should be mapped by Kriging predictor model at

2   ω_k, denoted by:

$$R_k = \eta_{re}^{(k)}\left(\boldsymbol{\theta}^*\right) \tag{28a}$$

$$T_k = \eta_{tr}^{(k)}\left(\boldsymbol{\theta}^*\right) \tag{28b}$$

5   The details of Kriging surrogate model are omitted and interested readers are referred to [53].

6   The formulated algorithm is shown in Table 1.

7   **3.3 Formulation of Bayesian inference for damage identification**

8   Based on the probabilistic model for scattering coefficients introduced in Section 3.1, the

9   coefficients predicted by the physics-rich model containing the parameters to be updated and

10 the experimentally measured scattering properties can be connected statistically. On the basis

11 of such connections, the likelihood function will be formulated hereby. Based on the

12 framework of Bayesian system identification [35], the posterior distribution can be achieved

13 by incorporating the prior information of the updated parameters and the likelihood function.

14   As is derived in the Appendix A, the variances of the FFT coefficient of the reflected

15 wave signal and the transmitted wave can be approximated by:

$$\sigma_{re}^2 = \sigma_{in}^2 \left(R_k^2(\boldsymbol{\theta}) + \gamma_{re} \right) \tag{29a}$$

$$\sigma_{tr}^2 = \sigma_{in}^2 \left(T_k^2(\boldsymbol{\theta}) + \gamma_{tr} \right) \tag{29b}$$

18 where $\sigma_{in}^2 = \mathrm{var}\left(X_{in}\right)$, $\sigma_{re}^2 = \mathrm{var}\left(X_{re}\right)$ and $\sigma_{tr}^2 = \mathrm{var}\left(X_{tr}\right)$ denote the variations of the incident

19 wave, the reflected wave and the transmitted wave, respectively; γ_{re} and γ_{tr} denote the

20 variances of the prediction errors of reflection and transmission coefficients; $R_k(\boldsymbol{\theta}) = \eta_{re}^{(k)}(\boldsymbol{\theta})$

1 and $T_k(\mathbf{\theta})=\eta_{tr}^k(\mathbf{\theta})$ denote the computed reflection and transmission coefficients at $\mathbf{\theta}$, which

2 are predicted by using the Kriging model introduced in Section 3.2.

3   As a result, substituting Eq. (29) into Eq.(7) and Eq. (8) leads to

$$p_{\Re_k}\left(r_k\middle|\mathbf{\theta},\gamma_{re}\right)=\frac{2r_k\left(R_k^2(\mathbf{\theta})+\gamma_{re}\right)}{\left(R_k^2(\mathbf{\theta})+\gamma_{re}+r_k^2\right)^2} \tag{30a}$$

$$p_{\Im_k}\left(\varepsilon_k\middle|\mathbf{\theta},\gamma_{tr}\right)=\frac{2\varepsilon_k\left(T_k^2(\mathbf{\theta})+\gamma_{tr}\right)}{\left(T_k^2(\mathbf{\theta})+\gamma_{tr}+\varepsilon_k^2\right)^2} \tag{30b}$$

6 Conditioned on the set of measurements $\mathcal{D}=\left\{\Re_k,\Im_k\middle|k=k_1,\cdots k_2\right\}$ formed over $\wp\in[k_1\Delta\omega,k_2\Delta\omega]$,

7 the likelihood function is given by

$$p\left(\Re_\wp\middle|\mathbf{\theta},\gamma_{re}\right)=\prod_{k=k_1}^{k_2}p_{\Re_k}\left(r_k\middle|\mathbf{\theta},\gamma_{re}\right)=\prod_{k=k_1}^{k_2}\frac{2r_k\left(R_k^2(\mathbf{\theta})+\gamma_{re}\right)}{\left(R_k^2(\mathbf{\theta})+\gamma_{re}+r_k^2\right)^2} \tag{31a}$$

$$p\left(\Im_\wp\middle|\mathbf{\theta},\gamma_{tr}\right)=\prod_{k=k_1}^{k_2}p_{\Im_k}\left(\varepsilon_k\middle|\mathbf{\theta},\gamma_{tr}\right)=\prod_{k=k_1}^{k_2}\frac{2\varepsilon_k\left(T_k^2(\mathbf{\theta})+\gamma_{tr}\right)}{\left(T_k^2(\mathbf{\theta})+\gamma_{tr}+\varepsilon_k^2\right)^2} \tag{31b}$$

10 According to the Bayes' theorem shown in Eq. (1), we can condition the prior on the training

11 data and integrate over the prior distribution of the coefficients to obtain the posterior

12 uncertainties of $\lambda=\left\{\mathbf{\theta},\gamma_{tr}\right\}$:

$$p\left(\lambda\middle|\mathfrak{M},\mathcal{D}\right)=p\left(\lambda\middle|\mathfrak{M}\right)\exp\left(-L(\lambda)\right) \tag{32}$$

14 with $L(\lambda)$ denoting the negative-log likelihood function given by

$$L(\lambda)=\sum_{k=k_1}^{k_2}\ln\frac{2r_k\left(R_k^2(\mathbf{\theta})+\gamma_{re}\right)}{\left(R_k^2(\mathbf{\theta})+\gamma_{re}+r_k^2\right)^2}+\sum_{k=k_1}^{k_2}\ln\frac{2\varepsilon_k\left(T_k^2(\mathbf{\theta})+\gamma_{tr}\right)}{\left(T_k^2(\mathbf{\theta})+\gamma_{tr}+\varepsilon_k^2\right)^2} \tag{33}$$

16 As a result, the posterior distribution $p\left(\lambda\middle|\mathfrak{M},\mathcal{D}\right)$ of the damage identification parameters and

17 prediction-error parameters can be achieved using TMCMC algorithm [39].

4 Step-by-step description of the Proposed Methodology

2   The proposed methodology is outlined below and its flowchart is shown in Fig. 6:

3 (a) Determine the scattering coefficients for the structure under investigation by GW

4   measurements:

5 • Excite the damaged structure and measure the incident wave $x_{in}(t)$, reflected wave $x_{re}(t)$

6   and transmitted wave $x_{tr}(t)$;

7 • Take FFT for incident wave $x_{in}(t)$, reflected wave $x_{re}(t)$ and transmitted wave $x_{tr}(t)$ to

8   obtain $X_{in}(\omega_k)$, $X_{re}(\omega_k)$ and $X_{tr}(\omega_k)$;

9 • Estimate scattering coefficients $\Re_k$ and $\Im_k$ by taking the absolute ratio of FFT of

10   reflected/transmitted wave (i.e., $X_{re}(\omega_k)$ and $X_{tr}(\omega_k)$) and that of incident wave $X_{in}(\omega_k)$;

11 (b) Construct Kriging surrogate model to numerically compute the relationship between the

12   scattering coefficients and the damage characterization parameters $\boldsymbol{\theta}$:

13 • Generate the sampling points of the parameters $\boldsymbol{\Theta} = \left\{ \boldsymbol{\theta}^{(1)}, \boldsymbol{\theta}^{(2)} \cdots \boldsymbol{\theta}^{(n_s)} \right\}^T$ using the proposed

14   experiment design strategy;

15 • Compute the reflection coefficients $\mathbf{Y}_{re}^{(i)}(\omega_k)$ and transmission coefficients $\mathbf{Y}_{tr}^{(i)}(\omega_k)$ at

16   each sample input $\boldsymbol{\theta}^{(i)}$ using the hybrid WFE formulation introduced in Section 3.2.1;

17 • Construct the Kriging model $R_k = \eta_{re}^{(k)}(\boldsymbol{\theta})$ and $T_k = \eta_{tr}^k(\boldsymbol{\theta})$ from the training set

18      $\mathcal{D}_{re} = \left(\boldsymbol{\Theta}, \mathbf{Y}_{re}(\omega_k) \right)$ and $\mathcal{D}_{tr} = \left(\boldsymbol{\Theta}, \mathbf{Y}_{tr}(\omega_k) \right)$ to predict the reflection and transmission

19   coefficients at any input $\boldsymbol{\theta}^*$;

20 (c) Formulate the likelihood function with the scattering coefficient estimates and those

1   predicted by the surrogate model in tandem with WFE according to Section 3.3;

2   (d) Calculate the posterior uncertainty of $\boldsymbol{\theta}$ with TMCMC.
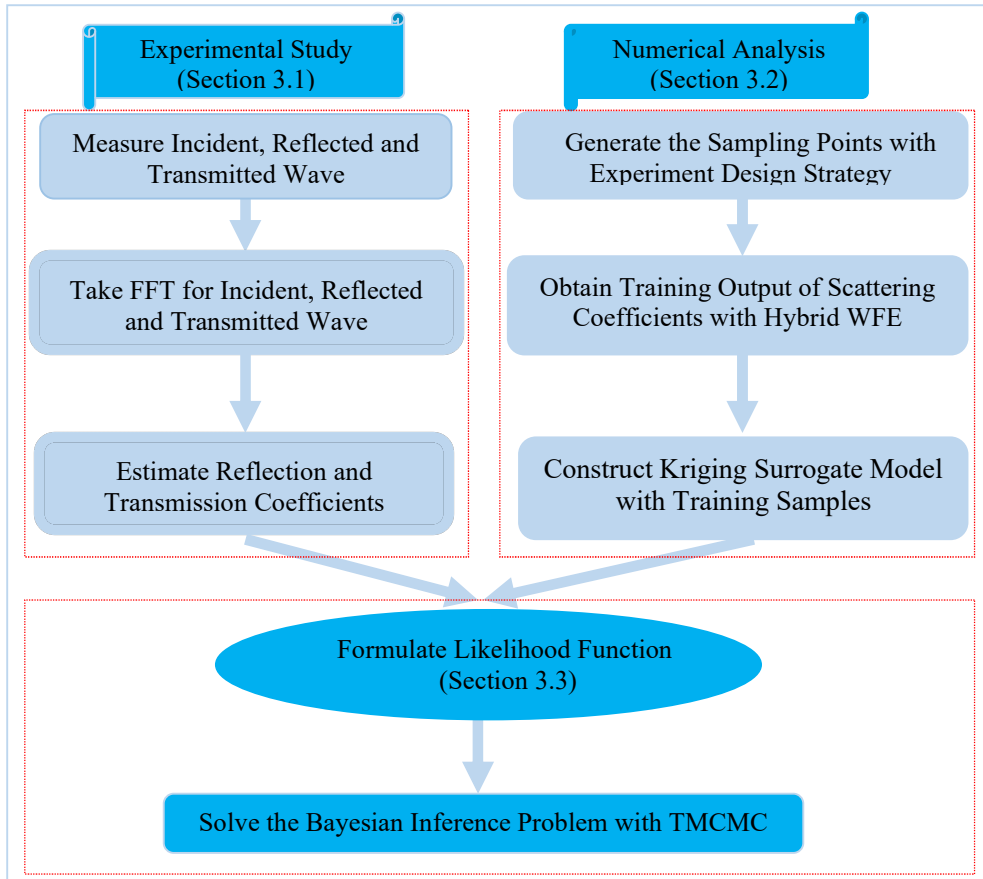
4   Fig. 6: Flowchart of the Bayesian inference for damage characterization with scattering

5   coefficients estimates and hybrid WFEM scheme

1   **5. Case Studies**

2   *5.1 Numerical validation: 3-D beam structure*
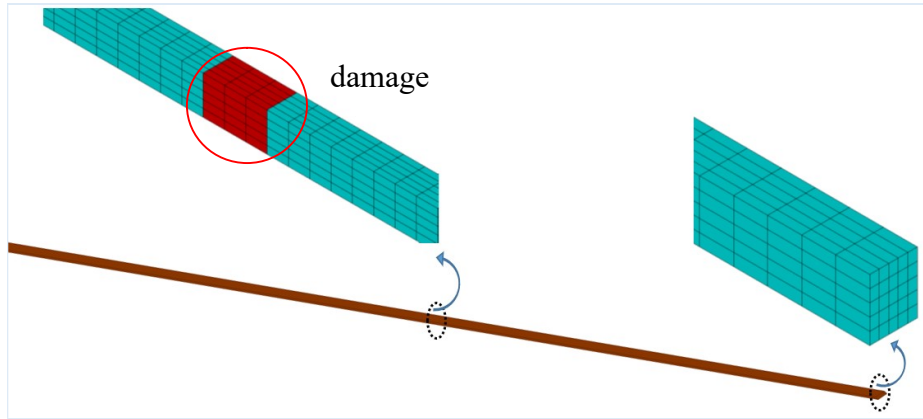
3

4   Fig. 7: The FE model of the 3-D beam, depicting the damaged coupling element in an

5   arbitrary position within the beam, as well as a portion of the healthy waveguide showing the

6   cross-sectional meshing employed in order to accurately capture the full wave basis

7   (including higher order Lamb modes) in a broadband sense

8   The numerical case study refers to a 3D beam structure modelled through brick, solid

9   linear elastic FEs. Simulated data of a 3-D beam shown in Fig. 7 are processed to further

10   illustrate the computational efficiency of the proposed Bayesian inference algorithm. In this

11   case,   the   Young's   modulus $E = 70\text{GPa}$;   the   area   of   the   cross   section

12   $A = 0.0009\text{m} \times 0.0007\text{m} = 6.3 \times 10^{-7}\,\text{m}^2$;   the   density   of   the   mass $\bar{m} = 3 \times 10^3\,\text{kg/m}^3$ are   the

13   characteristics of the healthy parts of the beam. In the presented case, linear, 8-node 3D

14   elements have been employed throughout the validation case studies. ANSYS (SOLID185)

15   was used for formulating the mass, stiffness and damping matrices for the structures. The

16   element size is 0.5mm, which is about 20 times smaller than the smallest desired wavelength

1   to be captured. Damage is assumed to occur in the middle of the beam. The mass and stiffness

2   matrices of the healthy waveguide are denoted by $\mathbf{K}_{und}$ and $\mathbf{M}_{und}$, respectively. For the

3   damage scenario, the stiffness scaling factors and mass scaling factor are introduced to model

4   the damaged element, i.e., $\mathbf{K}_d = \alpha \mathbf{K}_{und}$ and $\mathbf{M}_d = \rho \mathbf{M}_{und}$. For the damage scenario, it is

5   assumed that $\alpha = 0.5$ and $\rho = 1$.

6

7   (a)   (b)

8
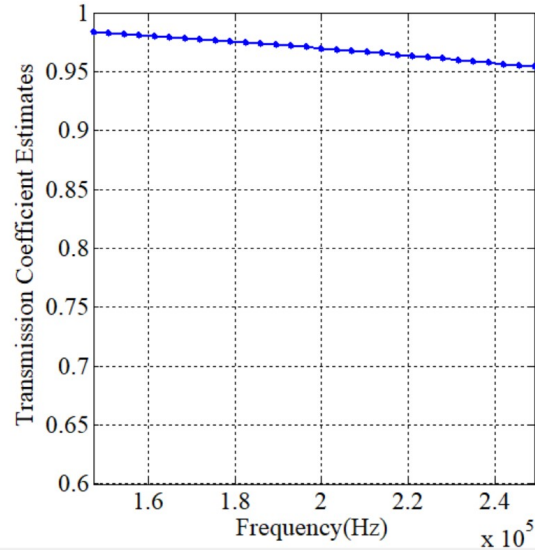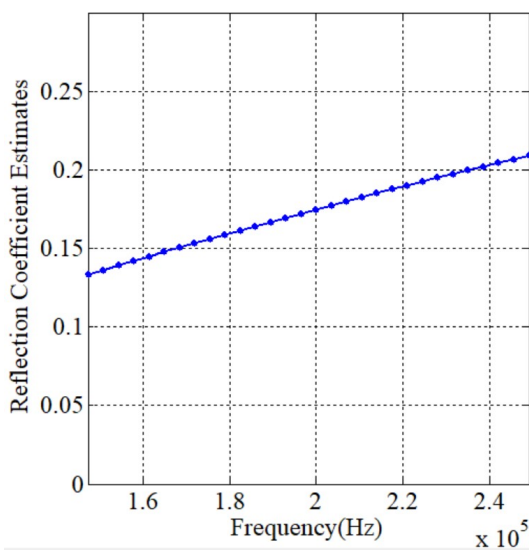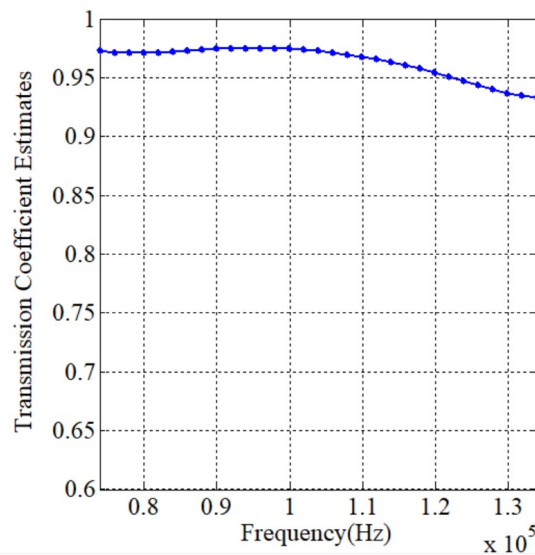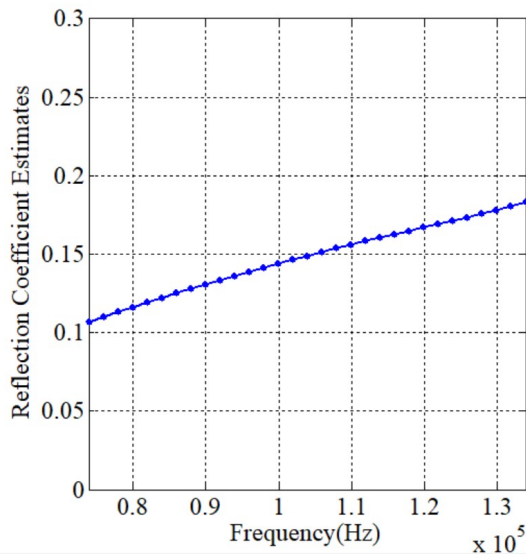
9   (c)   (d)

1 Fig. 8: Pseudo-experimental, explicit FE results obtained for (a) the reflection coefficients

2   for the longitudinal mode; (b) the transmission coefficients for the longitudinal mode; (c)

3   the reflection coefficients for the torsional mode; (d) the transmission coefficients for the

4   torsional mode. There results will later be injected within Bayesian inference scheme in

5   order to identify the damage characteristics that they represent.

6

7 The beam is excited by a 5-cycle Hanning-windowed sinusoidal tone burst with the

8 central frequency of 200 kHz. The desired modes including the longitudinal mode, torsional

9 mode and bending mode are generated by modeling the effect of piezoelectric actuators on the

10 beam. The incident wave, reflected wave and transmitted wave corresponding to different

11 modes are simulated using full, explicit FE modelling. Based on the explicit simulations, the

12 acquired reflection and transmission coefficients for the longitudinal (S_0), torsional (T_0) and

13 bending (A_0) modes can be estimated; the scattering coefficients of the first two modes are

14 illustrated in Fig. 8. It is worth noting again that the obtained scattering coefficients are

15 frequency-dependent, and only the frequency band around the excitation central frequency

16 $[150, 250]\,\mathrm{kHz}$ will be utilized for damage identification.

17 The parameters $\alpha = 0.5$ and $\rho = 1$ are left as unknowns to be determined through the

18 Bayesian estimation, i.e., the parameter set to be identified includes $\lambda = \{\alpha, \rho, \gamma_{in}, \gamma_{tr}\}$. Before

19 statistically inferring these parameters, the surrogate approximation between the scattering

20 coefficients and damage characterization parameters $\boldsymbol{\theta} = \{\alpha, \rho\}$ should be realized. The

21 possible ranges of parameters are set to be $[0.5\alpha, 1.5\alpha]$ and $[0.5\rho, 1.5\rho]$. A thousand samples

1 of $\boldsymbol{\theta}=\{\alpha,\rho\}$ were generated as training points. The hybrid WFE is built using 8-node 3D

2 linear elastic hexahedral element, leading to 432 DoFs for the damaged coupling element and

3 216 DoFs for the damage segment and the waveguide, respectively. The hybrid WFEM is run

4 for each training point to obtain the scattering coefficients of different dispersion modes at

5 different discrete frequencies within $[150,250]\text{kHz}$, yielding two vectors with each one

6 composed of thousands of training data outputs. With these sampling points and training

7 outputs at hand, the Kriging predictor models are formed at each frequency point ω_k .

8   Table 2: Identified results for the 3-D beam

Parameters	TMCMC assisted by Surrogate Approximation			TMCMC without using Surrogate Approximation		
	MPV	Mean	c.o.v. (%)	MPV	Mean	c.o.v. (%)
α	0.5105	0.511	0.18	0.508	0.509	0.22
ρ	1.003	1.002	0.33	1.008	1.006	0.38
γ_{in}	0.0008	0.00075	12.80	0.0007	0.0007	14.75
γ_{tr}	0.00243	0.023	11.47	0.0162	0.0169	15.53
Time	1249.7 s			15855.8 s		

9   Based on the surrogate model and the pseudo-experimental scattering coefficients, the

10 Bayesian approach is utilized for inferring the posterior distribution of $\lambda=\{\alpha,\rho,\gamma_{in},\gamma_{tr}\}$. The

11 prior distributions of updating parameters are all taken to be of uniform distribution. The

12 bound of stiffness scaling factor is equal to $[0.5\alpha,1.5\alpha]$, while the bound of the mass scaling

13 factor is assumed to be $[0.9\rho,1.1\rho]$. It is worth noting that the variation of ρ is taken to be

14 small so as to avoid making the identification problem ill-conditioned when treating α and ρ

15 as uncertain variables simultaneously.

1   By setting the TMCMC parameters to be $tolCov = 0.1$ and $N_j = 1000$, the Bayesian

2   inference takes 13 stages to achieve the posterior uncertainties, and the sampling points at

3   different stages are indicated in Fig. 9. The scatterplot matrices of $\lambda = \{\alpha, \rho, \gamma_{in}, \gamma_{tr}\}$ are

4   present in Fig. 10 as a 4×4 plot matrix. Diagonal plots indicate the marginal distributions of

5   the model parameters. The plots above/below the diagonal in Fig. 10 can indicate the

6   correlation between two parameters. From the projections in the α and ρ space, the

7   uncertainties in the α and ρ are strongly correlated. This result is consistent with the

8   intuition that the mass parameter and stiffness parameter are strongly correlated. Table 2

9   summarizes the results for simple measures such as the mean, the MPV and the c.o.v. of

10    $\lambda = \{\alpha, \rho, \gamma_{in}, \gamma_{tr}\}$. It is obvious that the mean is very close to the exact results, and the

11   standard deviation of the marginal distribution of the model parameters is very small.

12

13   (a)   (b)   (c)

14

15   (d)   (e)   (f)
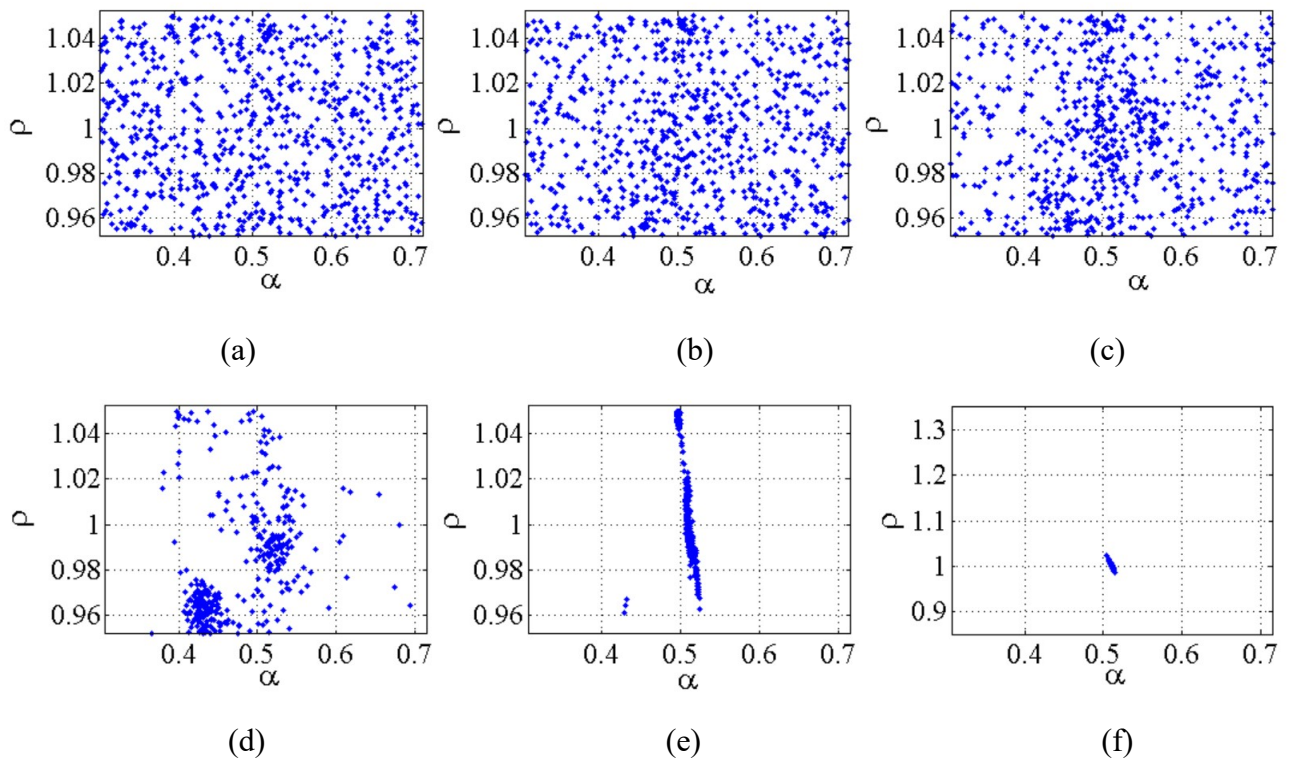
1　　Fig. 9: Convergence diagram of stochastic samples in the plane of $\{\alpha, \rho\}$ at different stages in

2　　Bayesian inference for damage detection of the 3-D beam using TMCMC: (a) stage 1; (b)

3　　stage 2; (c) stage 3; (d) stage 5; (e) stage 10; (f) stage 13.
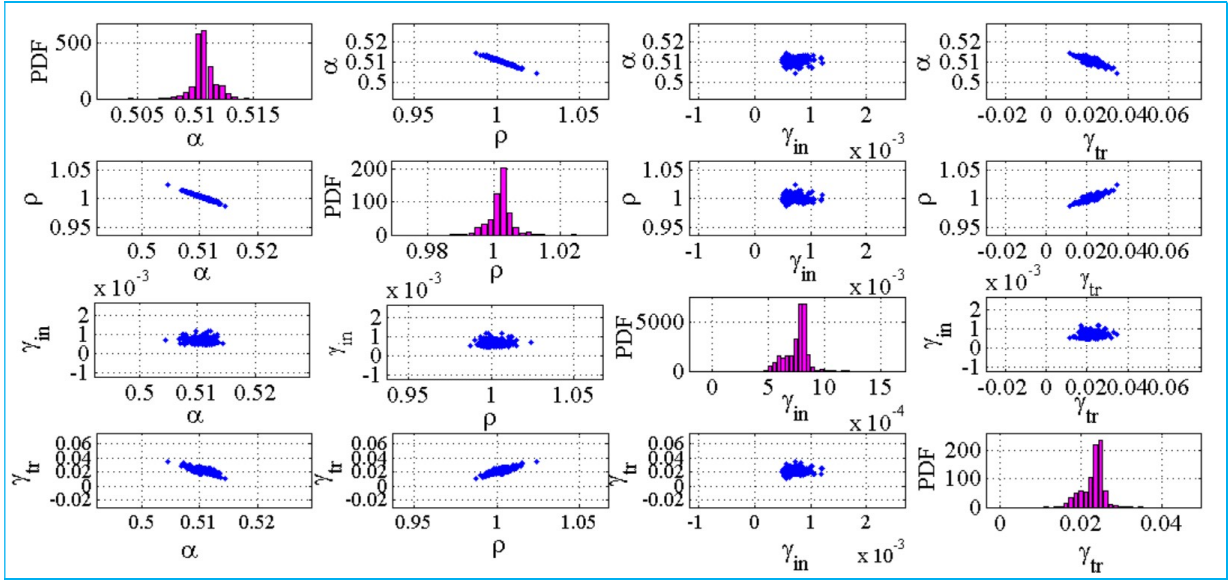
5　　Fig. 10: Scatterplot matrices of the identified parameters of the 3-D beam. Diagonal plots

6　　indicate the marginal distributions of the model parameters.

7

8　　　　The advantage of the proposed methodology in computational efficiency is next

9　　demonstrated by comparing the time costs for the cases with/without using hybrid WFEM

10　　scheme and surrogate model. We performed the Bayesian inference problem for all scenarios

11　　on a multicore server with Intel® Xeon® W-2123 Processor (8.25M Cache, 3.60 GHz) and

12　　32GB of RAM. In this case study, there are 432 DoFs and 216 DoFs for the damage segment

13　　and the waveguide. It would cost us around 1000s to build the surrogate model with WFE

14　　scheme. The time consumption of TMCMC assisted by Kriging model is around 1024

15　　seconds, while TMCMC without using surrogate model cost us more than 15000s and the

1   corresponding results are compared in Table 2. If explicit FE simulations without using

2   hybrid WFEM are employed for Bayesian inference, it is highly non-trivial to achieve the

3   results. For this 1-D wave propagation case, the time consumed by explicit FE method is

4   around 1300 times of that cost by hybrid WFE scheme in each run. As a result, the

5   computational efforts and the required memory space will increase explosively compared

6   with hybrid WFEM scheme as one has to carry out a large number of runs of full FE scheme

7   in stochastic simulation, with each run involving the calculation of the scattering coefficients

8   at different frequencies. For more complicated structures and multiple damage scenarios, the

9   curse of the computational burden will be even worse. Thus, compared with explicit FE

10   solution, using surrogate approximation and hybrid WFE scheme can lead to a drastic

11   reduction in the computational effort, without sacrificing in accuracy.

12   **5.2 Experimental verification using a composite beam with a crack**

13   To investigate the feasibility of the proposed method in real applications, a carbon fiber strip

14   shown in Fig. 11 was tested in the laboratory. The geometry dimensioning of the specimen is

15   950mm (length) × 7.7mm (width) × 1.0mm (thickness). The beam was tested without damage

16   and with a crack (the width $W=2.0mm$ and the depth $D=3.2mm$ measured by caliper) to

17   obtain the wave propagation velocity properties, as well as the scattering coefficients. The

18   sketched dimensions of the beam and the configuration of different piezoelectric (PZT)

19   sensors can be observed in Fig. 12. It is worth mentioning here that the details of the material

1   are unknown and we will estimate the wave propagation characteristics from the experimental

2   measurements.

3
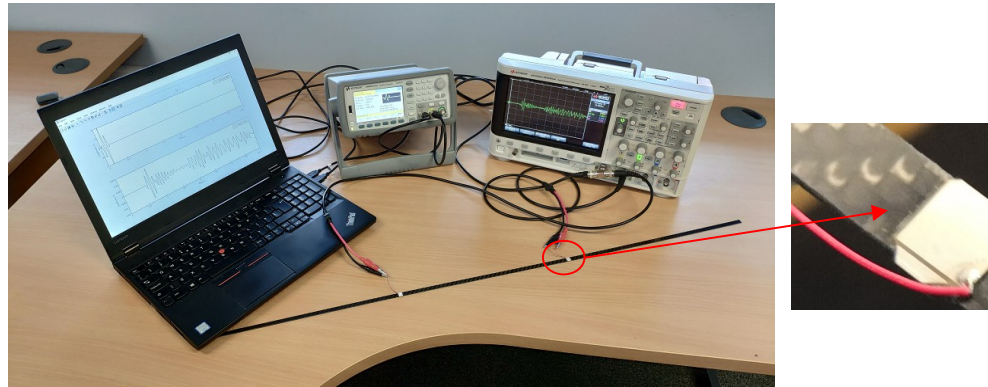
5   Fig. 11: Experimental suite used comprised of a laptop, an arbitrary waveform generator, and

6   an oscilloscope

7

8
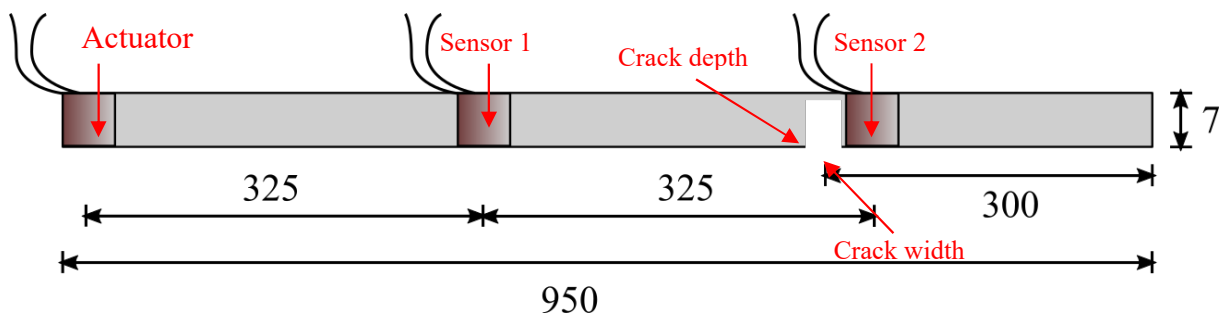
10   Fig. 12: Damage position and transducer locations within the carbon fiber strip (dimensions in

11   mm)

12

13   In the experimental test, one PZT was placed on the left end of the beam serving as the

14   actuator while the other two PZTs serves as sensors in a pitch-catch configuration.

15   Specifically, the specimen was excited with an ultrasonic sine-burst centered at different

16   frequencies (from 50kHz-250kHz with a step frequency of 10 kHz) with each scenario

17   consisting of 3 cycles and 8 Vpp amplitude, using a Keysight 33512B arbitrary waveform

1   generator. The guided waves registered in the sensor transducers were acquired by a

2   DSOX2014A oscilloscope applying a sampling frequency of 9.6 MHz. Each of these

3   measurements corresponds to the average of 32 individual measurements, to reduce random

4   noise. Regarding the piezo ceramic transducers, a rectangular width mode vibration type of

5   transducer (Steminc part number: SMPL7W8T02412WL) was selected to principally excite

6   elastic waves in the length direction, in order for edge reflections to be minimized.

7   For the ultrasonic GW testing, the first symmetric (S0) GW type was fully identified at

8   different frequencies from 50 kHz to 250 kHz with a step frequency of 10 kHz. The S_0 mode

9   propagation velocity, at various frequencies, was obtained based on the measurements of the

10   undamaged carbon strip before the data are processed for damage characterization.

11   Considering that the S_0 mode is non-dispersive, the calculation consisted on measuring the

12   first minimum peak of the wave packet, subtracting both time of flights and dividing the

13   distance between sensors by this time of flight difference as

14                                  $$V_{S_0} = d/\Delta t \qquad\qquad (34)$$

15   where d and Δt denote the distance between two sensors and the time of flight difference

16   which is indicated in Fig. 13(a). The considered distance is $d = 325mm$, and it is measured

17   from center to center of the PZT transducers. The velocity of the wave corresponding to

18   different excitation central frequencies is shown in Fig. 13(b). Based on the velocity, the

19   Young's modulus for the tested beam can be calibrated according to the theory presented in

20   [11], and their values are estimated as $70Gpa$. The density of the beam is also tested by

21   measuring the weight and the volume, and the calibrated density is $\rho=1.29kg/m^3$.

(a)

(b)
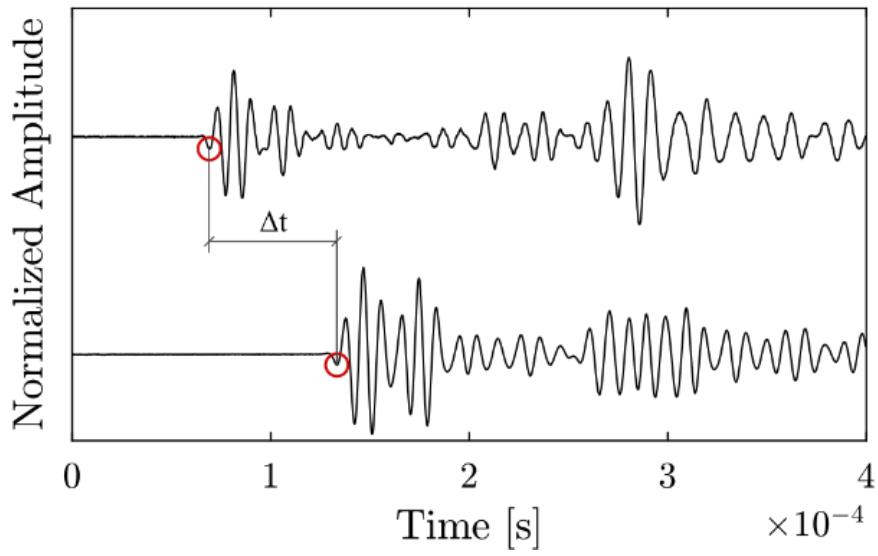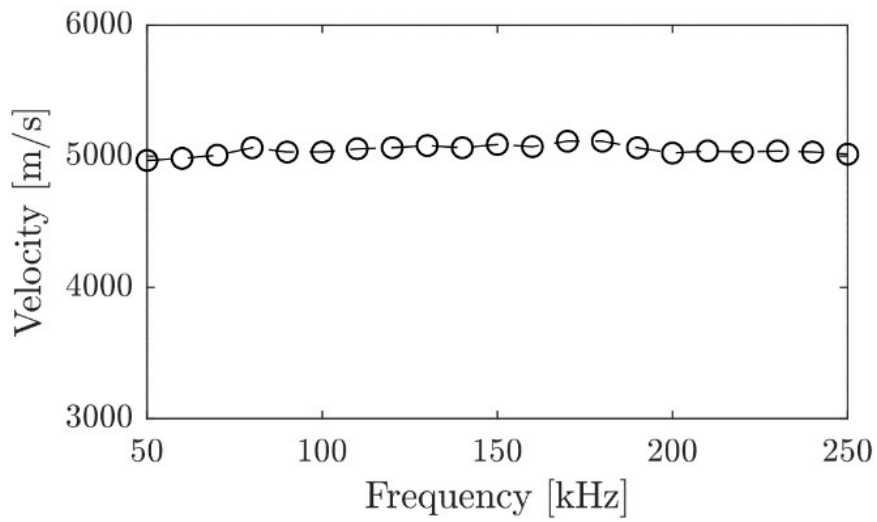
Fig. 13: Signals obtained by both sensor transducers at 100kHz showed in (a) and the wave propagation velocities obtained for the S_0 mode at different frequencies following the same method in (b)

1

2   (a)   (b)
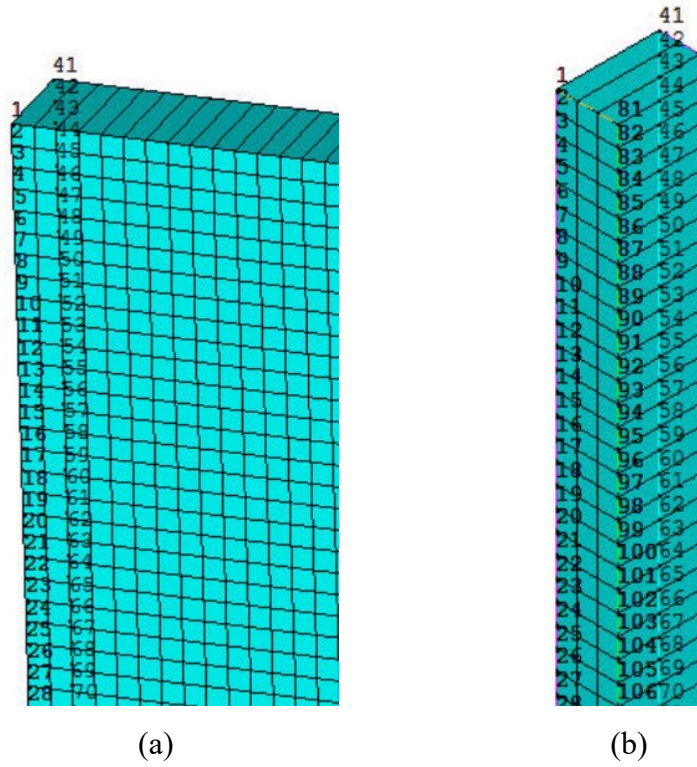
3   Fig. 14: FEM of the damaged carbon strip (a) and periodic elastic waveguide (b).

4

5

6

7
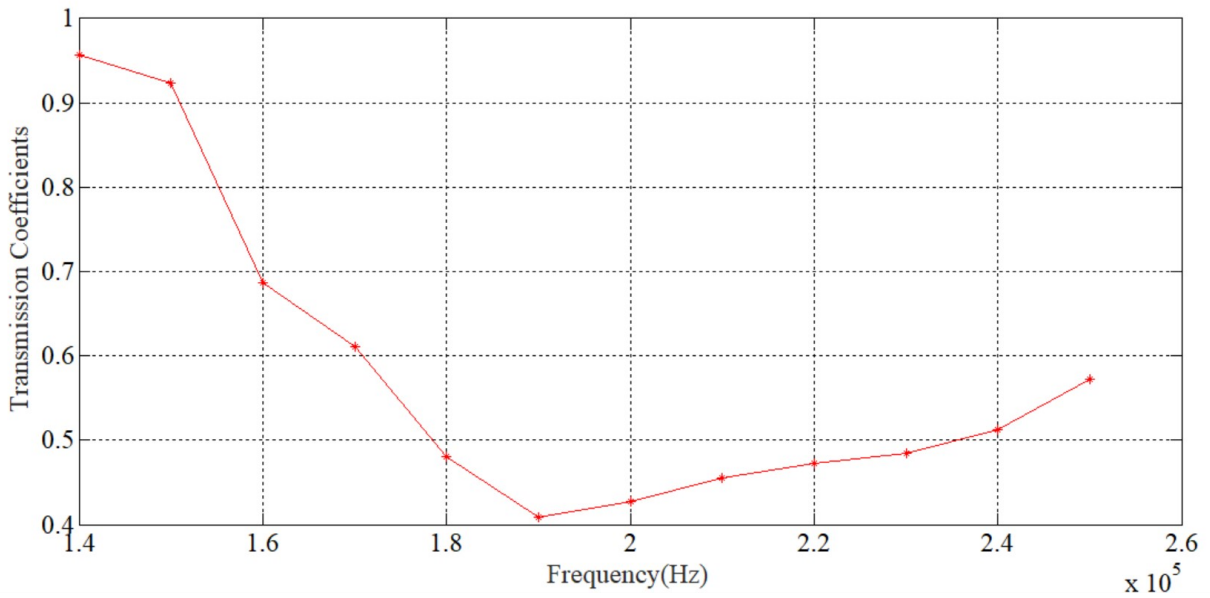
8   Fig. 15: Transmission coefficients estimated using the first symmetric (S0) GW signals

9   excited at different frequencies from 140 kHz to 250 kHz with a step frequency of 10 kHz.

10

1   In this study, the DoE training points for W and D are generated as training samples

2   using LHD. In each computer experiment, the numerical predictions of the transmission

3   coefficients at different frequencies are calculated using the hybrid WFE scheme. The training

4   data is then used for constructing the Kriging model reflecting the mathematical relationship

5   between transmission coefficients and the crack parameters $\{W, D\}$. The damaged coupling

6   element could exhibit complex mechanical behaviour through damage inconsistencies and is

7   fully modelled using solid 3D element in ANSYS. The FE models of the damaged segment

8   and the waveguide are illustrated in Fig. 14. The damaged segment includes thousands of

9   DoFs, varying for different training points due to the variation of the crack width and depth.

10   The waveguide includes 480 DoFs. Given that no surrogate model is used, the manipulation of

11   high dimensional DSMs at a number of frequencies can rule out Bayesian approaches due to

12   the expense of carrying out huge number of runs in stochastic simulations.

13   The acquired responses at "Sensor 2" with a crack were processed. The first crack-

14   scattered wave component, is the transmitted S_0 mode. The incident wave and the transmitted

15   wave were processed to determine the measured transmission coefficients. The transmission

16   coefficients corresponding to different frequencies are presented in Fig. 15; these will be used

17   to identify the crack size including the width W and the depth D. The parameter set to be

18   identified includes $\{W, D, \gamma_{tr}\}$. A uniform prior distribution was used with bounds

19   $[0.8mm, 5mm] \times [0.5mm, 3.5mm]$ for $\{W, D\}$ and $[0.05, 0.25]$ for the prediction-error parameter

20   γ_{tr}. Using the posterior samples from the last stage of TMCMC, we proceed to calculate the

21   uncertainty in some representative parameters. The mean values and the c.o.v. are presented

1   in Table 3. These values are also compared with the crack size measured by calipers in the

2   second column of Table 3. Fig. 16 presents the 3×3 scatterplot matrices of $\{W, D, \gamma_{tr}\}$. The

3   c.o.v. values of different parameters are of different orders of magnitude.

4   Table 3: Identified results of the composite beam

Parameters	Measured values	Identified values		
		Mean	Variance	c.o.v. (%)
D (mm)	3.20	3.61	0.278	7.697
W (mm)	1.98	1.75	0.872	49.835
γ_{tr}	-	0.1553	0.0326	21.026

5
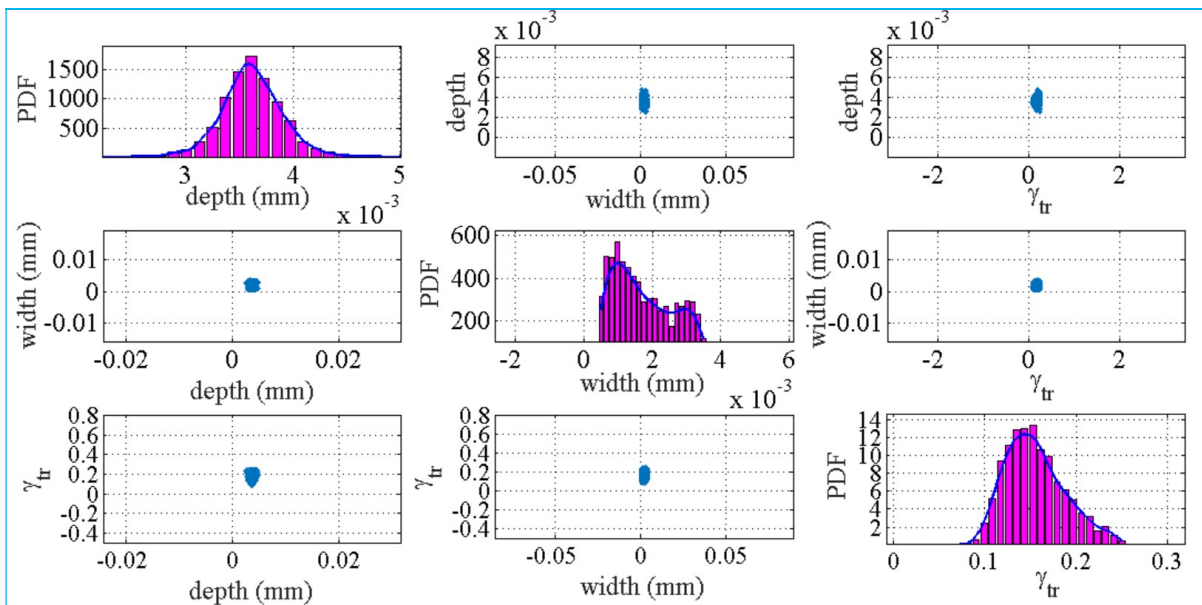
7   Fig. 16: Scatterplot matrices of different parameters of the composite beam. Diagonal plots

8   indicate the marginal distributions of the model parameters.

9

10   As observed from Table 3 and Fig. 16, the calibration procedure yields a reasonable

11   capture of the distribution function. However, there is still discrepancy between the identified

12   crack size and the measured crack size. The differences are attributable to the model error

1   associated with the inconsistencies between the ideal structural model in FEM and the

2   practical specimen in experiment, such as differences in damping and dispersion, and

3   differences in crack shape and the actual one. More specifically, the posterior c.o.v. of the

4   depth is much smaller than that of the width, indicating that the depth can be identified with

5   higher accuracy. Finally, it is important to highlight the main limitations of this approach. It

6   has potential issues as it is dependent on the damage model of the structure and the scattering

7   properties measurements. If the transmission coefficients cannot be estimated correctly

8   through physics-based approaches, or if several GW modes are mixed together, then the

9   presented methodology can become computationally unbearable. One of our future endeavors

10   is the employment of a 2D FFT within the identification scheme in order to simultaneously

11   work with several GW modes (this can be done individually with the exhibited scheme as it

12   currently stands).

13   **6 Concluding Remarks**

14   Ultrasonic GWs have played an important role in modern SHM technologies due to their high

15   sensitivity to small damage and early damage initiation. We hereby presented the first attempt

16   to investigate the possibility of using scattering coefficients for probabilistic damage

17   identification, through the uniqueness of GW interactions with each damage scenario. In the

18   context of damage detection with GWs, modelling error as well as measurement noise will

19   inevitably affects the results. This emphasizes the importance of using a comprehensive

20   statistical framework to account for the uncertainties in the parameters and their propagation

1   when in need for robust predictions consistent with experimental data. By making full use of

2   the Bayesian system identification framework to account for measurement noise and

3   modeling errors, this study aims at formulating a new, generic framework for probabilistic

4   damage identification. This is achieved by integrating a hybrid WFEM scheme employed for

5   scattering coefficient estimates, a Kriging predictor model as well a TMCMC stochastic

6   simulation technique. The following conclusions are drawn from the presented study:

7   ● Defined as the ratio of Fourier transform of two measurements, the measured scattering

8   coefficients can be well modeled as an absolute complex Gaussian ratio random variable

9   with concise and explicit closed-form solutions. As a result, one can embed the

10   "deterministic" structural damage characterization models within the class of probability

11   model of scattering properties, so that the damage identification models give a predictable

12   ("systematic") part and the prediction error is modeled as an uncertain ("random") part in

13   the statistical inference problem. The likelihood function connecting the scattering

14   properties predicted by the physics-rich scheme and the scattering coefficient estimates is

15   formulated within a Bayesian system identification framework, while the TMCMC is

16   utilized to sample the posterior PDF of the updated parameters.

17   ● The stochastic simulation becomes prohibitively expensive, and the difficulty in

18   interfacing different software environment (e.g., stochastic simulation toolbox in

19   MATLAB) with the FE analysis package (e.g., ANSYS) can limit the applicability of the

20   proposed probabilistic damage characterization algorithm. Kriging surrogate modelling

21   provides a surrogate mapping between the probability spaces of the damage parameters to

be identified and the model predictions of scattering coefficients; it is thus capable of replacing the extensive FE simulations required in the likelihood evaluations by very fast approximate estimates.

- To create a Kriging predictor model, an experiment design strategy which generates samples referenced as the training set is required. For each training point, the hybrid WFE approach is employed to predict the numerical predictions for scattering coefficients. The hybrid WFE is proved to be approximately 1,300 times faster than explicit FE simulations, therefore rendering the presented identification strategy feasible. The method relies on post-processing a standard FE model of a small segment of each waveguide using periodic structure theory. The models for the periodic healthy waveguide and the one of the damaged joining elements are coupled to yield the scattering matrices for the considered damage scenario.

- The accuracy and efficiency of the proposed methodology are validated by using the responses of one numerical example and one experimental study. The TMCMC assisted by surrogate model in tandem with the hybrid WFE can obtain satisfactory results with similar accuracy but save much computational effort and enhance the operability significantly, without resorting to interfacing different software. Results also show that we are able to identify damage in experimental scenarios, even with unknown material characteristics, but with a lower precision compared to the numerical case.

- Compared with the time domain approaches, the frequency domain approach has unique features. First, the scattering coefficients as frequency-dependent quantities in nature

have very clear physical meaning, which can describe the quantitative relationship between wave scattering and damage intensity. Furthermore, the frequency domain approaches are more computationally efficient than the time domain approaches, as the FFT coefficients at different frequencies are independently distributed [36,38], which indicates the likelihood function can be formulated more efficiently by multiplying the PDF at different frequency points directly, while one ought to estimate the covariance matrix among the outputs corresponding to different time for the time domain approaches. In addition, scattering coefficients working in the frequency domain can utilize data to selected bandwidths to legitimately control the excitation frequency and exclude the information from the noise spectrum.

● As a feasibility study, it is worth mentioning that the algorithm proposed in this study is not devoid of problems. As an example, wave mode conversion can take place when a GW impinges on the damage interface. While this phenomenon can actually increase the richness of information acquired for the present damage, it becomes computationally demanding to consider all conversion combinations and extract robust conclusions out of them. This is however a future research direction of intense interest. How to propagate the damage uncertainties due to mode conversion is, again, a future endeavor.

1 Acknowledgments

9

10 Appendix A: the variances of the reflection and transmission coefficients

11 In the context of Bayesian inference with scattering coefficients, the measured outputs and the

12 numerical model outputs are connected as follows:

$$\Re_k = R_k(\boldsymbol{\theta}) + \mu_{re} \tag{A1}$$

$$\Im_k = T_k(\boldsymbol{\theta}) + \mu_{tr} \tag{A2}$$

15 Based on the Kriging predictor model introduced in Section 3.2.2, the prediction of scattering

16 coefficients at different frequency points at $\boldsymbol{\theta}$ is given by

$$R_k = \eta_{re}^{(k)}(\boldsymbol{\theta}) \tag{A3}$$

$$T_k = \eta_{tr}^{k}(\boldsymbol{\theta}) \tag{A4}$$

19 Eq.(A1) and (A2) can be rearranged as

$$\left| \frac{X_{re}(\omega_k)}{X_{in}(\omega_k)} \right| = \eta_{re}^{(k)}(\boldsymbol{\theta}) + \mu_{re} \tag{A5}$$

$$\left|\frac{X_{tr}\left(\omega_k\right)}{X_{in}\left(\omega_k\right)}\right| = \eta_{tr}^{(k)}(\theta) + \mu_{tr}. \tag{A6}$$

As a result, one has

$$\left|X_{re}\right| = \left|X_{in}\right|\left[\eta_{re}^{(k)}(\theta) + \mu_{re}\right] \tag{A7}$$

$$\left|X_{tr}\right| = \left|X_{in}\right|\left[\eta_{tr}^{(k)}(\theta) + \mu_{tr}\right]. \tag{A8}$$

From (A4), one can obtain the variances of X_{re} and X_{tr} as follows:

$$\mathrm{var}\left(X_{re}\right) = \mathrm{var}\left(X_{in}\right)\left[\left(\eta_{re}^{(k)}(\theta)\right)^2 + \mathrm{var}\left(\mu_{re}\right)\right] \tag{A9}$$

$$\mathrm{var}\left(X_{tr}\right) = \mathrm{var}\left(X_{in}\right)\left[\left(\eta_{tr}^{(k)}(\theta)\right)^2 + \mathrm{var}\left(\mu_{tr}\right)\right]. \tag{A10}$$

In real applications, it is usually assumed that the variation of the prediction error are

constants, i.e., $\gamma_{re} = \mathrm{var}\left(\mu_{re}\right)$ and $\gamma_{tr} = \mathrm{var}\left(\mu_{tr}\right)$. By denoting that $\sigma_{in}^2 = \mathrm{var}\left(X_{in}\right)$, $\sigma_{re}^2 = \mathrm{var}\left(X_{re}\right)$,

$\sigma_{tr}^2 = \mathrm{var}\left(X_{tr}\right)$, (A5) can be expressed as:

$$\sigma_{re}^2 = \sigma_{in}^2\left(\left(\eta_{re}^{(k)}(\theta)\right)^2 + \gamma_{re}\right) \tag{A11}$$

$$\sigma_{tr}^2 = \sigma_{in}^2\left(\left(\eta_{tr}^{(k)}(\theta)\right)^2 + \gamma_{tr}\right) \tag{A12}$$

References

[1] C.R. Farrar, K. Worden, An introduction to structural health monitoring, Philosophical

Transactions of the Royal Society of London A: Mathematical, Physical and Engineering

Sciences 365 (1851) (2007) 303-315.

[2] P. Cawley, Structural health monitoring: Closing the gap between research and industrial

deployment, Structural Health Monitoring 17(5) (2018)1225-44.

[3] E. Reynders, G.D. Roeck, Reference-based combined deterministic-stochastic subspace

identification for experimental and operational modal analysis, Mechanical Systems and Signal Processing 22 (3) (2008) 617-637.

[4] H.F. Lam, T. Yin, Statistical detection of multiple cracks on thin plates utilizing dynamic response, Engineering Structures 32 (10) (2010) 3145-3152.

[5] D. Montalvao, N.M.M. Maia, A.M.R. Ribeiro, A review of vibration-based structural health monitoring with special emphasis on composite materials, Shock and Vibration Digest 38 (4) (2006) 295-324.

[6] V. Giurgiutiu, A. Zagrai, J.J. Bao, Piezoelectric wafer embedded active sensors for aging aircraft structural health monitoring, Structural Health Monitoring 1 (1) (2002) 41-61.

[7] Y.K. An, H. Sohn, Integrated impedance and guided wave based damage detection, Mechanical Systems and Signal Processing 28 (2012) 50-62.

[8] Z. Su, L. Ye, Y. Lu, Guided Lamb waves for identification of damage in composite structures: A review, Journal of Sound and Vibration 295 (3-5) (2006) 753-780.

[9] B.C. Lee, W.J. Staszewski, Sensor location studies for damage detection with Lamb waves, Smart Materials and Structures 16 (2) (2007) 399-408.

[10] S. Torkamani, S. Roy, M.E. Barkey, E. Sazonov, S. Burkett, S. Kotru, A novel damage index for damage identification using guided waves with application in laminated composites, Smart Materials and Structures 23 (9) (2014) 095015.

[11] D. Chronopoulos, C. Droz, R. Apalowo, M. Ichchou, W.J. Yan, Accurate structural identification for layered composite structures, through a wave and finite element scheme, Composite Structures 182 (2017) 566-578.

[12] J.M. Renno, B.R. Mace, Calculation of reflection and transmission coefficients of joints using a hybrid finite element/wave and finite element approach, Journal of Sound and Vibration 332 (9) (2013) 2149-2164.

[13] G. Mitrou, N. Ferguson, J. Renno, Wave transmission through two-dimensional structures by the hybrid FE/WFE approach, Journal of Sound and Vibration 389 (2017) 484-501.

[14] Y. Lu, L. Ye, Z. Su, C. Yang, Quantitative assessment of through-thickness crack size based on Lamb wave scattering in aluminium plates, Ndt & E International 41 (1) (2008) 59-68.

[15] B. Hosten, L. Moreau, M. Castaings, Reflection and transmission coefficients for guided waves reflected by defects in viscoelastic material plates, The Journal of the Acoustical Society of America 121 (6) (2007) 3409-3417.

[16] M. Krawczuk, M. Palacz, A. Zak, W.M. Ostachowicz, Transmission and reflection coefficients for damage identification in 1D elements, Key Engineering Materials 413 (2009) 95-100.

[17] O. Diligent, T. Grahn, A. Boström, P. Cawley, M.J.S. Lowe, The low-frequency reflection and scattering of the S0 Lamb mode from a circular through-thickness hole in a plate: finite element, analytical and experimental studies, The Journal of the Acoustical Society of America 112 (6) (2002) 2589-601.

[18] M.J.S. Lowe, Characteristics of the reflection of Lamb waves from defects in plates and pipes, Review of Progress in Quantitative Nondestructive Evaluation, Springer, Boston, MA (1998) 113-120.

[19] A. Demma, P. Cawley, M.J.S. Lowe, A.G. Roosenbrand, The reflection of the fundamental torsional mode from cracks and notches in pipes, The Journal of the Acoustical Society of America 114 (2) (2003) 611-25.

[20] E.B. Flynn, M.D. Todd, P.D. Wilcox, B.W. Drinkwater, A.J. Croxford, Maximum-likelihood estimation of damage location in guided-wave structural health monitoring, Proceedings of the Royal Society of London A: Mathematical, Physical and Engineering Sciences 467 (2133) (2011) 2575-2596.

[21] L. Qiu, S. Yuan, Q. Bao, H. Mei, Y. Ren, Crack propagation monitoring in a full-scale aircraft fatigue test based on guided wave-Gaussian mixture model, Smart Materials and Structures 25 (5) (2016) 055048.

[22] C.T. Ng, M. Veidt, H.F. Lam, Guided wave damage characterisation in beams utilising probabilistic optimisation, Engineering Structures 31 (12) (2009) 2842-2850.

[23] O.A. Vanli, S. Jung, Statistical updating of finite element model with Lamb wave sensing data for damage detection problems, Mechanical Systems and Signal Processing 42 (1-2) (2014) 137-151.

[24] G. Yan, A Bayesian approach for damage localization in plate-like structures using Lamb waves, Smart Materials and Structures 22 (3) (2013) 035012.

[25] G. Yan, H. Sun, H. Waisman, A guided Bayesian inference approach for detection of multiple flaws in structures using the extended finite element method, Computers & Structures 152 (2015) 27-44.

[26] C.T. Ng, Bayesian model updating approach for experimental identification of damage in

beams using guided waves, Structural Health Monitoring 13 (4) (2014) 359-373.

[27] C.T. Ng, On the selection of advanced signal processing techniques for guided wave damage identification using a statistical approach, Engineering Structures 67 (2014) 50-60.

[28] S. He, C.T. Ng, A probabilistic approach for quantitative identification of multiple delaminations in laminated composite beams using guided waves, Engineering Structures 127 (2016) 602-614.

[29] S. He, C.T. Ng, Guided wave-based identification of multiple cracks in beams using a Bayesian approach, Mechanical Systems and Signal Processing 84 (2017) 324-345.

[30] A.B. Abdessalem, F. Jenson, P. Calmon, Quantifying uncertainty in parameter estimates of ultrasonic inspection system using Bayesian computational framework, Mechanical Systems and Signal Processing 109 (2018) 89-110.

[31] B. Wu, Y. Huang, X. Chen, S. Krishnaswamy, H. Li, Guided-wave signal processing by the sparse Bayesian learning approach employing Gabor pulse model, Structural Health Monitoring 16(3) (2017) 347-362.

[32] J. Chiachío, N. Bochud, M. Chiachío, S. Cantero, G. Rus, A multilevel Bayesian method for ultrasound-based damage identification in composite laminates, Mechanical Systems and Signal Processing 88 (2017) 462-477.

[33] J. Yang, J. He, X. Guan, D. Wang, H. Chen, W. Zhang, Y. Liu, A probabilistic crack size quantification method using in-situ Lamb wave test and Bayesian updating, Mechanical Systems and Signal Processing 78 (2016) 118-133.

[34] S. Cantero-Chinchilla, J. Chiachío, M. Chiachío, D. Chronopoulos, A. Jones, A robust Bayesian methodology for damage localization in plate-like structures using ultrasonic guided-waves, Mechanical Systems and Signal Processing 122 (2019) 192-205.

[35] J.L. Beck, L.S. Katafygiotis, Updating models and their uncertainties. I: Bayesian statistical framework, Journal of Engineering Mechanics, ASCE 124 (4) (1998) 455-461.

[36] K.V. Yuen, Bayesian methods for structural dynamics and civil engineering, John Wiley & Sons (2010).

[37] K.V. Yuen, S.C. Kuok, Bayesian methods for updating dynamic models, Applied Mechanics Reviews 64 (1) (2011) 010802.

[38] S.K. Au, Operational Modal Analysis: Modeling, Bayesian Inference, Uncertainty Laws, Springer (2017).

[39] J. Ching, Y.C. Chen, Transitional Markov chain Monte Carlo method for Bayesian model updating, model class selection, and model averaging, Journal of Engineering Mechanics 133 (7) (2007) 816-832.

[40] W.J. Yan, W.X. Ren, Circularly-symmetric complex normal ratio distribution for scalar transmissibility functions. Part I: Fundamentals, Mechanical Systems and Signal Processing 80 (2016) 58-77.

[41] W.J. Yan, W.X. Ren, Circularly-symmetric complex normal ratio distribution for scalar transmissibility functions. Part II: probabilistic model and validation, Mechanical Systems and Signal Processing 80 (2016) 78-98.

[42] W.J. Yan, W.X. Ren, Generalized proper complex Gaussian ratio distribution and its

application to statistical inference for frequency response functions, Journal of Engineering Mechanics, ASCE 144 (9) (2018) 04018080.

[43] E. Simoen, C. Papadimitriou, G. Lombaert, On prediction error correlation in Bayesian model updating, Journal of Sound and Vibration 332(18) (2013) 4136-4152.

[44] E.L. Zhang, P. Feissel, J. Antoni, A comprehensive Bayesian approach for model updating and quantification of modeling errors, Probabilistic Engineering Mechanics 26(4) (2011) 550-560.

[45] S.H. Cheung, J.L. Beck, Bayesian model updating using hybrid Monte Carlo simulation with application to structural dynamic models with many uncertain parameters, Journal of Engineering Mechanics 135 (4) (2009) 243-255.

[46] J.L. Beck, S.K. Au, Bayesian updating of structural models and reliability using Markov chain Monte Carlo simulation, Journal of Engineering Mechanics 128 (4) (2002) 380-391.

[47] R.K. Apalowo, D. Chronopoulos, G. Tanner, Wave interaction with defects in pressurised composite structures, Journal of Nondestructive Evaluation 37 (3) (2018) 37-48.

[48] D. Chronopoulos, Calculation of guided wave interaction with nonlinearities and generation of harmonics in composite structures through a wave finite element method, Composite Structures 186 (2018) 375-384.

[49] G. Matheron, Principles of geostatistics, Economic Geology 58 (1963) 1246.

[50] J.P.C. Kleijnen, Kriging metamodeling in simulation: A review, European Journal of Operational Research 192 (3) (2009) 707-716.

[51] S.N. Lophaven, H.B. Nielsen, J. Søndergaard, DACE: a Matlab kriging toolbox (Vol. 2),

IMM, Informatics and Mathematical Modelling, The Technical University of Denmark (2002).

[52] J. Zhang, F.T.K Au, Calibration of initial cable forces in cable-stayed bridge based on Kriging approach, Finite Elements in Analysis and Design 92 (2014) 80-92.

[53] M. Balesdent, J. Morio, J. Marzat, Kriging-based adaptive importance sampling algorithms for rare event estimation, Structural Safety 44 (2013) 1-10.

[54] I. Kaymaz, Application of kriging method to structural reliability problems. Structural Safety 27(2) (2005) 133-151.

[55] P.E. Hadjidoukas, P. Angelikopoulos, C. Papadimitriou, P. Koumoutsakos, Π4U: A high performance computing framework for Bayesian uncertainty quantification of complex models, Journal of Computational Physics 284 (2015) 1-21.

[56] P. Angelikopoulos, C. Papadimitriou, P. Koumoutsakos, X-TMCMC: Adaptive kriging for Bayesian inverse modeling, Computer Methods in Applied Mechanics and Engineering 289 (2015) 409-428.